

## Article

# Electron Impact Excitation of Extreme Ultra-Violet Transitions in $\text{Xe}^{7+}$ – $\text{Xe}^{10+}$ Ions

Aloka Kumar Sahoo <sup>†</sup> and Lalita Sharma <sup>\*,†</sup>

Department of Physics, Indian Institute of Technology, Roorkee 247667, India; aloka\_s@ph.iitr.ac.in

\* Correspondence: lalita.sharma@ph.iitr.ac.in; Tel.: +91-1332-28-5729

† These authors contributed equally to this work.

**Abstract:** In the present work, a detailed study on the electron impact excitation of  $\text{Xe}^{7+}$ ,  $\text{Xe}^{8+}$ ,  $\text{Xe}^{9+}$  and  $\text{Xe}^{10+}$  ions for the dipole allowed (E1) transitions in the EUV range of 8–19 nm is presented. The multi-configuration Dirac–Fock method is used for the atomic structure calculation including the Breit and QED corrections along with the relativistic configuration interaction approach. We have compared our calculated energy levels, wavelengths and transition rates with other reported experimental and theoretical results. Further, the relativistic distorted wave method is used to calculate the cross sections from the excitation threshold to 3000 eV electron energy. For plasma physics applications, we have reported the fitting parameters of these cross sections using two different formulae for low and high energy ranges. The rate coefficients are also obtained using our calculated cross sections and considering the Maxwellian electron energy distribution function in the electron temperature range from 5 eV to 100 eV.

**Keywords:** MCDF wavefunctions; wavelengths; transition rates; relativistic distorted wave method; cross sections; rate coefficients



**Citation:** Sahoo, A.K.; Sharma, L. Electron Impact Excitation of Extreme Ultra-Violet Transitions in  $\text{Xe}^{7+}$ – $\text{Xe}^{10+}$  Ions. *Atoms* **2021**, *9*, 76. <https://doi.org/10.3390/atoms9040076>

Academic Editor: Grzegorz Piotr Karwasz

Received: 3 September 2021

Accepted: 30 September 2021

Published: 6 October 2021

**Publisher's Note:** MDPI stays neutral with regard to jurisdictional claims in published maps and institutional affiliations.



**Copyright:** © 2021 by the authors. Licensee MDPI, Basel, Switzerland. This article is an open access article distributed under the terms and conditions of the Creative Commons Attribution (CC BY) license (<https://creativecommons.org/licenses/by/4.0/>).

## 1. Introduction

Spectroscopic and collisional data of highly charged xenon ions in the extreme ultra-violet (EUV) spectral range play a vital role in several research areas. For example, laser produced xenon plasma exhibits [1] the possibility to become an EUV source for the next generation lithography. Xenon ions are detected in the UV spectrum of the astrophysical objects viz., hot DO-type white dwarf [2] and planetary nebula [3]. In the next generation fusion reactor ITER, xenon is expected to be used as edge plasma coolant. Xenon ions being used in ion thruster for electric propulsion [4] plays key role in making the modern space exploration cheaper. Since emissions from various charged species of xenon ions carry information about the plasma parameters and impurities, their atomic structure and dynamical properties in the EUV range are essential for the accurate diagnostics of the aforementioned plasmas. Therefore, in this work we have focused on the electron impact excitation of the electric dipole (E1) transitions in  $\text{Xe}^{7+}$ ,  $\text{Xe}^{8+}$ ,  $\text{Xe}^{9+}$  and  $\text{Xe}^{10+}$  ions in the EUV region 8–19 nm. We consider excitation of E1 transitions that are responsible for the most intense lines of the spectra.

To determine the emission properties of xenon ions, experiments have been performed with either laser or gas discharge-produced plasmas. Churilov and Joshi [5] recorded xenon spectra in the 7–17 nm region on a 10.7 m grazing incidence spectrograph and analyzed the  $4\text{p}^64\text{d}^9 - (4\text{p}^64\text{d}^85\text{p} + 4\text{p}^64\text{d}^84\text{f} + 4\text{p}^54\text{d}^{10})$  transition array of Rh-like  $\text{Xe}^{9+}$ . They also identified the resonance transitions arising from the excited  $4\text{d}^9(6\text{p} + 5\text{f} + 7\text{p} + 6\text{f})$  states of Pd-like  $\text{Xe}^{8+}$  and  $4\text{d}^{10}5\text{s}^2 - 4\text{d}^95\text{s}4\text{f}^2$  transitions for Ag-like  $\text{Xe}^{7+}$ . Churilov et al. [6] observed the transition array  $4\text{d}^8 - (4\text{d}^75\text{p} + 4\text{d}^74\text{f} + 4\text{p}^54\text{d}^9)$  of  $\text{Xe}^{10+}$  using a low inductance vacuum spark and a 10.7 m grazing incidence photograph in the EUV region 10.5–15.7 nm. These lines were analyzed using Hartree–Fock (HFR) calculations in relativistic mode with the help of the Cowan suite of codes [7]. Fahy et al. [8] reported the EUV spectra of

Xe<sup>6+</sup> to Xe<sup>41+</sup> in the wavelength region of 4.5 to 20 nm using the electron beam ion trap (EBIT) facility at NIST while varying electron beam energy from 180 eV to 8 keV. They also calculated the transition probabilities and wavelengths using the HF approximation with the Cowan code [7]. Ali and Nakamura [9] observed the EUV spectra of Rh-like Xe<sup>9+</sup>–Cd-like Xe<sup>6+</sup> and Cu-like Xe<sup>25+</sup>–Se-like Xe<sup>20+</sup> using a compact electron beam ion trap (CoBIT) and a flat-field grazing incidence spectrometer in the wavelength range of 15–20 nm with an uncertainty of 0.05 Å. The electron beam energy was varied between 200–890 eV during these measurements. Ali and Nakamura [10] also used their experimental facilities to record EUV spectra of highly charged Xe<sup>8+</sup>–Xe<sup>11+</sup> and Ba<sup>18+</sup>–Ba<sup>21+</sup> ions in the wavelength range 9–13 nm. Merabet et al. [11] studied spectra of various xenon ions (Xe<sup>2+</sup>–Xe<sup>10+</sup>) in the EUV region 10–16 nm using a compact electron cyclotron resonance ion source (CECRIS) equipped with a grazing monochromator operating in 4–90 nm.

Various theoretical studies have been carried out to report energy levels, wavelengths, oscillator strengths and transition probabilities of xenon ions. Safranova et al. [12] calculated the atomic properties of Pd-like ions Xe<sup>8+</sup> with nuclear charge ranging from Z = 47 to 100 using relativistic many-body perturbation theory (RMBPT) with Breit correction. Ivanova [13] used the relativistic perturbation theory with a model potential to calculate the energy levels of Ag-, Pd- and Rh-like ions with Z = 52–86. Motoumba et al. [14] reported transition probabilities and oscillator strengths for the transition array 4d<sup>8</sup> – (4p<sup>5</sup>4d<sup>9</sup> + 4d<sup>7</sup>5p + 4d<sup>7</sup>4f) of Xe<sup>10+</sup> in the EUV spectral range of 10.2–15.7 nm. These results were obtained using two different methods viz., the semi-empirical pseudo-relativistic Hartree–Fock (HFR) method and the relativistic multiconfiguration Dirac–Hartree–Fock (MCDHF) theory within the relativistic configuration interaction (RCI) approximation. Motoumba et al. [15] also employed the above two methods to report transition probabilities and oscillator strengths for 92 spectral lines of Xe<sup>9+</sup> ion in the range of 11–16.4 nm. Shen et al. [16] used Flexible Atomic Code (FAC), based on a fully relativistic approach, to calculate the energy levels, oscillator strengths, electron impact collision strengths as well as effective collision strengths for Xe<sup>10+</sup>.

It is clear from the above discussion that most of the previous experimental or theoretical studies on Xe<sup>7+</sup>–Xe<sup>10+</sup> ions have focused on their spectroscopic properties, while the electron impact cross section data are scarcely reported. However, various studies in the past have clearly demonstrated that using accurate cross section results in a collisional radiative model provides a better agreement with the measurements on the plasma parameters, *viz.*, electron temperature and density [17–20]. Therefore, reliable cross sections are essential for the success of any plasma model. In general, suitable theoretical methods are employed to carry out cross section calculations due to limitations, such as accurate identification of the fine-structure levels for open shell ions, in performing the scattering experiments.

In the present work, we have studied electron impact excitation of Xe<sup>7+</sup>, Xe<sup>8+</sup>, Xe<sup>9+</sup> and Xe<sup>10+</sup> ions. The core shell configuration (1s<sup>2</sup> 2s<sup>2</sup> 2p<sup>6</sup> 3s<sup>2</sup> 3p<sup>6</sup> 3d<sup>10</sup> 4s<sup>2</sup> 4p<sup>6</sup>) is removed in the representation of the ground and excited state configurations of these four ions. We have considered the transition arrays 4d<sup>10</sup>5s 2S<sub>1/2</sub>–(4d<sup>9</sup>5s4f + 4d<sup>9</sup>5s5p) for Xe<sup>7+</sup>, 4d<sup>10</sup>1S<sub>0</sub>–(4d<sup>9</sup>5p + 4d<sup>9</sup>4f + 4d<sup>9</sup>6p + 4d<sup>9</sup>5f + 4d<sup>9</sup>7p + 4d<sup>9</sup>6f) for Xe<sup>8+</sup>, 4p<sup>6</sup>4d<sup>9</sup>–(4p<sup>6</sup>4d<sup>8</sup>5p + 4p<sup>6</sup>4d<sup>8</sup>4f + 4p<sup>5</sup>4d<sup>10</sup>) for Xe<sup>9+</sup> and 4d<sup>8</sup>–(4d<sup>7</sup>5p + 4d<sup>7</sup>4f + 4p<sup>5</sup>4d<sup>9</sup>) for Xe<sup>10+</sup>. These arrays result into 9, 18, 75 and 57 E1 transitions in Xe<sup>7+</sup> through Xe<sup>10+</sup> in EUV range. We have used multi-configuration Dirac–Fock method within RCI approximation to calculate the energy levels, wavelengths and transition rates. These results are compared in detail with the previously reported measurements and theoretical calculations. The target ion wavefunctions are further implemented in the evaluation of the transition (*T*–) matrix amplitude using relativistic distorted wave (RDW) approximation and excitation cross sections are obtained up to 3000 eV electron energy. The analytical fitting of the electron excitation cross sections is also performed as it is more convenient to feed the analytical expression with fitting parameters for plasma modeling. Further, assuming electron energy distribution to be

Maxwellian, we have also calculated excitation rate coefficients using our cross sections for electron temperature range 5–100 eV.

## 2. Theory

In order to calculate the energy levels, wavelengths and transition probabilities, we have obtained MCDF wavefunctions of  $\text{Xe}^{7+}$ – $\text{Xe}^{10+}$  ions using GRASP2K code [21]. In the MCDF method, the atomic state functions (ASFs) are written as linear combination of configuration state functions (CSFs) having same parity  $P$  and angular momentum quantum number  $J$ , as follows:

$$\Psi(PJM) = \sum_{i=1}^n a_i \Phi_i(PJM). \quad (1)$$

Here  $a_i$  refers to the mixing coefficient of the CSF  $\Phi_i(PJM)$  which are anti-symmetrized products of a common set of orthonormal orbitals. In our calculations, we take as many CSFs as are having at least 0.001% value of the mixing coefficient. The configurations that are included in the atomic-structure calculations of xenon ions are listed in Table 1. These configurations are shown here in their non-relativistic notations. The MCDF method implements a self-consistent field procedure for obtaining the radial functions and the mixing coefficients. Further, we performed RCI calculations by considering the Breit and quantum electrodynamic (QED) corrections in the Dirac–Coulomb Hamiltonian. The transition probabilities are computed from the matrix element of dipole operator of the electromagnetic field.

**Table 1.** Configurations of the initial and final states and the CSFs in non-relativistic notations.

Ions	Initial State	Final State		CSFs
$\text{Xe}^{7+}$	$4\text{d}^{10}5\text{s}$	$4\text{d}^9(5\text{s}5\text{p}, 4\text{f}5\text{s})$	even	$4\text{d}^{10}(5\text{s}, 5\text{d}, 6\text{s}, 6\text{d}),$ $4\text{d}^9(5\text{s}5\text{d}, 5\text{s}6\text{s}, 5\text{s}7\text{s},$ $5\text{s}^2, 5\text{p}^2)$
			odd	$4\text{d}^{10}(4\text{f}, 5\text{p}, 6\text{p}),$ $4\text{d}^9(4\text{f}5\text{s}, 5\text{s}5\text{p}, 5\text{s}5\text{f},$ $5\text{s}6\text{f}, 5\text{p}5\text{d})$
$\text{Xe}^{8+}$	$4\text{d}^{10}$	$4\text{d}^9(4\text{f}, 5\text{p}, 5\text{f}, 6\text{p}, 6\text{f}, 7\text{p})$	even	$4\text{d}^{10}, 4\text{d}^9(5\text{s}, 5\text{d}, 6\text{s}, 6\text{d},$ $7\text{s}, 7\text{d}), 4\text{d}^8(5\text{s}^2, 5\text{p}^2,$ $5\text{d}^2)$
			odd	$4\text{d}^9(4\text{f}, 5\text{p}, 5\text{f}, 6\text{p}, 6\text{f}, 7\text{p},$ $7\text{f})$
$\text{Xe}^{9+}$	$4\text{d}^9$	$4\text{d}^8(4\text{f}, 5\text{p}), 4\text{p}^54\text{d}^{10}$	even	$4\text{d}^9, 4\text{d}^8(5\text{s}, 5\text{d}, 6\text{s}, 6\text{d},$ $7\text{s}, 7\text{d}), 4\text{p}^54\text{d}^9(5\text{p}, 5\text{f}),$ $4\text{d}^7(5\text{s}^2, 5\text{p}^2, 5\text{d}^2, 5\text{f}^2,$ $5\text{s}5\text{d}, 5\text{s}6\text{s}, 5\text{s}6\text{d}, 5\text{p}5\text{f})$
			odd	$4\text{d}^8(4\text{f}, 5\text{p}, 5\text{f}, 6\text{p}, 6\text{f},$ $7\text{p}), 4\text{d}^7(5\text{s}5\text{p}, 5\text{s}5\text{f},$ $5\text{s}6\text{p}), 4\text{p}^54\text{d}^{10}, 4\text{d}^64\text{f}^3$
$\text{Xe}^{10+}$	$4\text{d}^8$	$4\text{d}^7(4\text{f}, 5\text{p}), 4\text{p}^54\text{d}^9$	even	$4\text{d}^8, 4\text{d}^75\text{d}, 4\text{p}^54\text{d}^8(5\text{p},$ $5\text{f}), 4\text{d}^6(5\text{s}^2 + 5\text{p}^2)$
			odd	$4\text{d}^7(4\text{f}, 5\text{p}, 5\text{f}, 6\text{f}),$ $4\text{p}^54\text{d}^9, 4\text{p}^54\text{d}^85\text{d},$ $4\text{d}^54\text{f}^3$

We further use the bound state wavefunctions of the ion in the relativistic distorted wave theory to determine the electron impact excitation parameters. The  $T$ -matrix in the

RDW approximation for excitation of an  $N$  electron ion from an initial state  $a$  to a final state  $b$  can be written as [22]:

$$T_{a \rightarrow b}^{RDW}(\gamma_b, J_b, M_b, \mu_b; \gamma_a, J_a, M_a, \mu_a) = \langle \chi_b^- | V - U_b(N+1) | \mathcal{A} \chi_a^+ \rangle. \quad (2)$$

Here,  $J_{a(b)}$ ,  $M_{a(b)}$  denote the total angular momentum quantum number and its associated magnetic quantum number in the initial(final) state, whereas,  $\gamma_{a(b)}$  represents additional quantum numbers required for unique identification of the state.  $\mu_{a(b)}$  refers to the spin projection of the incident(scattered) electron.  $\mathcal{A}$  is the anti-symmetrization operator to consider the exchange of the projectile electron with the target electrons and  $U_b$  is the distortion potential which is taken to be a function of the radial co-ordinates of the projectile electron only. In our calculations, we choose  $U_b$  to be a spherically averaged static potential of the excited state of ion. In the above Equation (2),  $V$  is the Coulomb interaction potential between the incident electron and the target ion. The wave function  $\chi_{a(b)}^{+(-)}$  represents the product of the  $N$ -electron target wave functions  $\Psi_{a(b)}$  and a projectile electron distorted wave function  $F_{a(b)}^{+(-)}$  in the initial ' $a$ ' and final ' $b$ ', states, that is:

$$\chi_{a(b)}^{+(-)} = \Psi_{a(b)}(1, 2, \dots, N) F_{a(b)}^{+(-)}(k_{a(b)}, N+1). \quad (3)$$

Here, '+(-)' sign denotes an outgoing(incoming) wave, while  $k_{a(b)}$  is the linear momentum of the projectile electron in the initial(final) state. Equation (2) contains entire information about the excitation process. We, however, are interested in computing only the integrated cross section which is obtained by taking square of the mode value of the complex  $T$ -matrix with appropriate normalization, as expressed below:

$$\sigma_{a \rightarrow b} = (2\pi)^4 \frac{k_b}{k_a} \frac{1}{2(2J_a + 1)} \sum_{M_b \mu_b M_a \mu_a} \int |T_{a \rightarrow b}^{RDW}(\gamma_b, J_b, M_b, \mu_b; \gamma_a, J_a, M_a, \mu_a)|^2 d\Omega. \quad (4)$$

### 3. Results and Discussion

#### 3.1. Atomic-Structure Calculations

We have used GRASP2K code [21] to perform MCDF and RCI calculations to obtain energy levels, wavelengths and transition rates of  $Xe^{7+}$ – $Xe^{10+}$  ions. Our energy values are presented and compared with other theoretical and experimental results through Tables 2–5 for the four ions. The fine-structure states are represented in the relativistic  $j-j$  coupling scheme in which all shells, excluding  $s$ , split into two subshells with  $j = l \pm 1/2$ . For example, a  $p$  shell will be broken as  $\bar{p}$  with  $j = 1/2$  and  $p$  with  $j = 3/2$ . In order to identify the levels, their indices are assigned in each table. This will help to clearly recognise the states for which wavelengths, transition rates, electron impact cross sections and excitation rate coefficients will be presented.

**Table 2.** Comparison of our calculated energy levels (in eV) with other results for  $Xe^{7+}$ . A fully filled subshell is omitted in the relativistic representation of the configurations.

Index	State *	J	State	Present	NIST [23]
1	$4d^{10}s^2S_{1/2}$	1/2	$5s_{1/2}$	0.0000	0.0000
2	$4d^95s5p (5/2, ^3P_1)$	3/2	$(4d_{5/2}^5 5s_{1/2})_2 5\bar{p}_{1/2}$	66.2099	67.1436
3	$4d^95s5p (3/2, ^3P_0)$	3/2	$(4d_{3/2}^3 5s_{1/2})_1 5\bar{p}_{1/2}$	67.1423	68.2470
4	$4d^95s5p (3/2, ^3P_0)$	3/2	$(4d_{3/2}^3 5s_{1/2})_2 5\bar{p}_{1/2}$	68.1925	69.0120
5	$4d^95s5p (3/2, ^1P_1)$	1/2	$(4d_{3/2}^3 5s_{1/2})_1 5\bar{p}_{1/2}$	69.1417	69.9456
6	$4d^95s5p (3/2, ^3P_2)$	1/2	$(4d_{3/2}^3 5s_{1/2})_1 5p_{3/2}$	69.5680	70.4968
7	$4d^95s5p (5/2, ^1P_1)$	3/2	$(4d_{5/2}^5 5s_{1/2})_3 5p_{3/2}$	72.9254	72.5665
8	$4d^95s5p (3/2, ^1P_1)$	1/2	$(4d_{3/2}^3 5s_{1/2})_2 5p_{3/2}$	74.7061	74.3872
9	$4d^95s4f ^2P_{1/2}$	1/2	$(4d_{5/2}^5 4f_{7/2})_5 s_{1/2}$	103.5676	100.5830
10	$4d^95s4f ^2P_{3/2}$	3/2	$(4d_{5/2}^5 4f_{7/2})_1 s_{1/2}$	103.6716	100.6000

\* Notation as per the NIST [23] database.

**Table 3.** Same as Table 2 but for Xe<sup>8+</sup>.

Index	State *	J	State	Present	Other Reported
1	4d <sup>10</sup> 1S <sub>0</sub>	0	4d <sub>0</sub> <sup>6</sup>	0.0000	0.0000 <sup>a</sup>
2	4d <sup>9</sup> 5p 3P <sub>2</sub>	2	4d <sub>5/2</sub> <sup>5</sup> 5p <sub>1/2</sub>	71.0998	71.3452 <sup>b</sup>
3	4d <sup>9</sup> 5p 3P <sub>1</sub>	1	4d <sub>3/2</sub> <sup>3</sup> 5p <sub>1/2</sub>	73.4043	73.7114 <sup>a</sup>
4	4d <sup>9</sup> 5p 3P <sub>0</sub>	0	4d <sub>3/2</sub> <sup>3</sup> 5p <sub>3/2</sub>	74.9525	75.3707 <sup>b</sup>
5	4d <sup>9</sup> 5p 1P <sub>1</sub>	1	4d <sub>3/2</sub> <sup>3</sup> 5p <sub>1/2</sub>	75.0407	74.9951 <sup>a</sup>
6	4d <sup>9</sup> 5p 3D <sub>3</sub>	3	4d <sub>5/2</sub> <sup>5</sup> 5p <sub>3/2</sub>	74.9691	75.0613 <sup>b</sup>
7	4d <sup>9</sup> 5p 3D <sub>1</sub>	1	4d <sub>3/2</sub> <sup>3</sup> 5p <sub>3/2</sub>	76.5287	76.6556 <sup>a</sup>
8	4d <sup>9</sup> 5p 3D <sub>2</sub>	2	4d <sub>3/2</sub> <sup>3</sup> 5p <sub>3/2</sub>	76.8981	77.0124 <sup>b</sup>
9	4d <sup>9</sup> 4f 3P <sub>0</sub>	0	4d <sub>5/2</sub> <sup>4</sup> f <sub>5/2</sub>	81.5153	
10	4d <sup>9</sup> 4f 3P <sub>1</sub>	1	4d <sub>5/2</sub> <sup>4</sup> f <sub>5/2</sub>	81.8543	82.5053 <sup>a</sup>
11	4d <sup>9</sup> 4f 3P <sub>2</sub>	2	4d <sub>5/2</sub> <sup>4</sup> f <sub>7/2</sub>	82.5160	
12	4d <sup>9</sup> 4f 3D <sub>3</sub>	3	4d <sub>5/2</sub> <sup>4</sup> f <sub>5/2</sub>	85.4793	
13	4d <sup>9</sup> 4f 3D <sub>1</sub>	1	4d <sub>3/2</sub> <sup>4</sup> f <sub>5/2</sub>	86.1987	86.3315 <sup>a</sup>
14	4d <sup>9</sup> 4f 3D <sub>2</sub>	2	4d <sub>3/2</sub> <sup>4</sup> f <sub>7/2</sub>	86.4396	
15	4d <sup>9</sup> 4f 1P <sub>1</sub>	1	4d <sub>5/2</sub> <sup>4</sup> f <sub>7/2</sub>	106.6396	103.2057 <sup>a</sup>
16	4d <sup>9</sup> 6p 3P <sub>2</sub>	2	4d <sub>5/2</sub> <sup>6</sup> p <sub>1/2</sub>	117.0829	
17	4d <sup>9</sup> 6p 3P <sub>1</sub>	1	4d <sub>5/2</sub> <sup>6</sup> p <sub>3/2</sub>	118.2765	119.4365 <sup>a</sup>
18	4d <sup>9</sup> 6p 3P <sub>0</sub>	0	4d <sub>3/2</sub> <sup>6</sup> p <sub>3/2</sub>	119.8886	
19	4d <sup>9</sup> 6p 1P <sub>1</sub>	1	4d <sub>3/2</sub> <sup>6</sup> p <sub>1/2</sub>	119.4555	120.5896 <sup>a</sup>
20	4d <sup>9</sup> 6p 3D <sub>3</sub>	3	4d <sub>5/2</sub> <sup>6</sup> p <sub>3/2</sub>	118.5929	
21	4d <sup>9</sup> 6p 3D <sub>1</sub>	1	4d <sub>3/2</sub> <sup>6</sup> p <sub>3/2</sub>	120.3813	121.4157 <sup>a</sup>
22	4d <sup>9</sup> 6p 3D <sub>2</sub>	2	4d <sub>3/2</sub> <sup>6</sup> p <sub>3/2</sub>	120.5895	
23	4d <sup>9</sup> 5f 3P <sub>0</sub>	0	4d <sub>5/2</sub> <sup>5</sup> f <sub>5/2</sub>	122.3364	
24	4d <sup>9</sup> 5f 3P <sub>1</sub>	1	4d <sub>5/2</sub> <sup>5</sup> f <sub>5/2</sub>	122.5205	123.0839 <sup>a</sup>
25	4d <sup>9</sup> 5f 3P <sub>2</sub>	2	4d <sub>5/2</sub> <sup>5</sup> f <sub>7/2</sub>	122.7973	
26	4d <sup>9</sup> 5f 3D <sub>1</sub>	1	4d <sub>5/2</sub> <sup>5</sup> f <sub>7/2</sub>	124.0985	124.5409 <sup>a</sup>
27	4d <sup>9</sup> 5f 3D <sub>3</sub>	3	4d <sub>5/2</sub> <sup>5</sup> f <sub>5/2</sub>	123.3075	125.8984 <sup>b</sup>
28	4d <sup>9</sup> 5f 3D <sub>2</sub>	2	4d <sub>3/2</sub> <sup>5</sup> f <sub>7/2</sub>	124.8695	
29	4d <sup>9</sup> 5f 1P <sub>1</sub>	1	4d <sub>3/2</sub> <sup>5</sup> f <sub>5/2</sub>	129.4696	128.5494 <sup>a</sup>
30	4d <sup>9</sup> 7p 3P <sub>2</sub>	2	4d <sub>5/2</sub> <sup>7</sup> p <sub>1/2</sub>	138.0878	
31	4d <sup>9</sup> 7p 3P <sub>1</sub>	1	4d <sub>3/2</sub> <sup>7</sup> p <sub>1/2</sub>	140.2617	140.1840 <sup>a</sup>
32	4d <sup>9</sup> 7p 3P <sub>0</sub>	0	4d <sub>3/2</sub> <sup>7</sup> p <sub>3/2</sub>	140.5323	
33	4d <sup>9</sup> 7p 1P <sub>1</sub>	1	4d <sub>5/2</sub> <sup>7</sup> p <sub>3/2</sub>	138.7018	141.6688 <sup>a</sup>
34	4d <sup>9</sup> 7p 3D <sub>3</sub>	3	4d <sub>5/2</sub> <sup>7</sup> p <sub>3/2</sub>	138.8464	
35	4d <sup>9</sup> 7p 3D <sub>1</sub>	1	4d <sub>3/2</sub> <sup>7</sup> p <sub>3/2</sub>	140.7750	142.2001 <sup>a</sup>
36	4d <sup>9</sup> 7p 3D <sub>2</sub>	2	4d <sub>3/2</sub> <sup>7</sup> p <sub>3/2</sub>	140.8804	
37	4d <sup>9</sup> 6f 3P <sub>0</sub>	0	4d <sub>5/2</sub> <sup>6</sup> f <sub>5/2</sub>	140.6424	
38	4d <sup>9</sup> 6f 3P <sub>1</sub>	1	4d <sub>5/2</sub> <sup>6</sup> f <sub>5/2</sub>	140.7218	142.0305 <sup>a</sup>
39	4d <sup>9</sup> 6f 3P <sub>2</sub>	2	4d <sub>5/2</sub> <sup>6</sup> f <sub>7/2</sub>	140.8523	
40	4d <sup>9</sup> 6f 3D <sub>3</sub>	3	4d <sub>5/2</sub> <sup>6</sup> f <sub>5/2</sub>	141.0695	
41	4d <sup>9</sup> 6f 3D <sub>1</sub>	1	4d <sub>5/2</sub> <sup>6</sup> f <sub>7/2</sub>	141.7116	142.9743 <sup>a</sup>
42	4d <sup>9</sup> 6f 3D <sub>2</sub>	2	4d <sub>3/2</sub> <sup>6</sup> f <sub>7/2</sub>	142.8798	
43	4d <sup>9</sup> 6f 1P <sub>1</sub>	1	4d <sub>3/2</sub> <sup>6</sup> f <sub>5/2</sub>	144.2122	145.1465 <sup>a</sup>

\* LS Coupling notation, <sup>a</sup>—Churilov and Joshi [5], <sup>b</sup>—NIST [23].

**Table 4.** Same as Table 2 but for Xe<sup>9+</sup>.

Index	Configuration	J	Level <sup>†</sup>	State	Present	Exp [5]	HFR [15]	MCDHF [15]
1	4d <sup>9</sup>	5/2	0	4d <sub>5/2</sub> <sup>5</sup>	0.0000	0.0000	0.0000	0.0000
2	4d <sup>9</sup>	3/2	16725	4d <sub>3/2</sub> <sup>3</sup>	2.0213	2.0736	2.0736	2.0485
3	4d <sup>8</sup> 5p	7/2	629040	4d <sub>4/2</sub> <sup>5</sup> 5p <sub>1/2</sub>	77.7037	77.9911	78.0033	77.0501
4	4p <sup>5</sup> 4d <sup>10</sup>	3/2	629234	4p <sub>3/2</sub> <sup>3</sup>	80.4530	78.0151	77.9893	79.0030
5	4d <sup>8</sup> 5p	3/2	644130	4d <sub>2/2</sub> <sup>5</sup> 5p <sub>1/2</sub>	79.8222	79.8620	79.8418	80.1652
6	4d <sup>8</sup> 5p	5/2	646494	(4d <sub>3/2</sub> <sup>3</sup> 4d <sub>5/2</sub> <sup>5</sup> ) <sub>3</sub> 5p <sub>1/2</sub>	79.9613	80.1551	80.1541	79.2899
7	4d <sup>8</sup> 5p	7/2	646880	(4d <sub>3/2</sub> <sup>3</sup> 4d <sub>5/2</sub> <sup>5</sup> ) <sub>3</sub> 5p <sub>1/2</sub>	79.9342	80.2029	80.1946	79.3275
8	4d <sup>8</sup> 5p	3/2	654245	(4d <sub>3/2</sub> <sup>3</sup> 4d <sub>5/2</sub> <sup>5</sup> ) <sub>2</sub> 5p <sub>1/2</sub>	80.9040	81.1161	81.1284	80.2543
9	4d <sup>8</sup> 5p	1/2	656520	4d <sub>0/2</sub> <sup>5</sup> 5p <sub>1/2</sub>	81.2487	81.3981	81.3843	80.5229
10	4d <sup>8</sup> 5p	5/2	657645	(4d <sub>3/2</sub> <sup>3</sup> 4d <sub>5/2</sub> <sup>5</sup> ) <sub>2</sub> 5p <sub>1/2</sub>	81.4372	81.5376	81.5389	80.7503
11	4d <sup>8</sup> 5p	7/2	658993	4d <sub>4/2</sub> <sup>5</sup> p <sub>3/2</sub>	81.5424	81.7048	81.7286	80.8887
12	4d <sup>8</sup> 5p	3/2	662160	(4d <sub>3/2</sub> <sup>3</sup> 4d <sub>5/2</sub> <sup>5</sup> ) <sub>2</sub> 5p <sub>1/2</sub>	82.0310	82.0974	82.1027	81.3059
13	4d <sup>8</sup> 5p	5/2	664256	4d <sub>4/2</sub> <sup>5</sup> p <sub>3/2</sub>	82.4106	82.3573	82.3841	81.7013
14	4d <sup>8</sup> 5p	5/2	668525	(4d <sub>3/2</sub> <sup>3</sup> 4d <sub>5/2</sub> <sup>5</sup> ) <sub>3</sub> 5p <sub>3/2</sub>	82.6723	82.8866	82.8941	82.0430
15	4d <sup>8</sup> 5p	7/2	669531	4d <sub>4/2</sub> <sup>5</sup> p <sub>3/2</sub>	82.9641	83.0113	83.0269	82.2869
16	4d <sup>8</sup> 5p	5/2	671045	4d <sub>2/2</sub> <sup>5</sup> p <sub>3/2</sub>	83.2829	83.1990	83.2350	82.5064
17	4d <sup>8</sup> 5p	7/2	672762	(4d <sub>3/2</sub> <sup>3</sup> 4d <sub>5/2</sub> <sup>5</sup> ) <sub>3</sub> 5p <sub>3/2</sub>	83.2202	83.4119	83.4178	82.5993
18	4d <sup>8</sup> 5p	3/2	674159	4d <sub>2/2</sub> <sup>5</sup> 5p <sub>1/2</sub>	83.5709	83.5851	83.5608	82.8836
19	4d <sup>8</sup> 5p	5/2	675652	4d <sub>2/2</sub> <sup>5</sup> p <sub>1/2</sub>	83.7487	83.7702	83.7698	83.0561
20	4d <sup>8</sup> 4f	7/2	676893	4d <sub>4/2</sub> <sup>4</sup> f <sub>5/2</sub>	83.7547	83.9241	83.9372	84.1222
21	4d <sup>8</sup> 5p	3/2	677421	(4d <sub>3/2</sub> <sup>3</sup> 4d <sub>5/2</sub> <sup>5</sup> ) <sub>1</sub> 5p <sub>1/2</sub>	84.1519	83.9895	83.9671	83.4135
22	4d <sup>8</sup> 5p	1/2	677704	4d <sub>2/2</sub> <sup>5</sup> p <sub>3/2</sub>	84.2510	84.0246	84.0003	83.5000
23	4d <sup>8</sup> 4f	5/2	678351	4d <sub>4/2</sub> <sup>4</sup> f <sub>5/2</sub>	83.9360	84.1048	84.0633	84.2632
24	4d <sup>8</sup> 5p	1/2	681425	4d <sub>2/2</sub> <sup>5</sup> p <sub>3/2</sub>	84.3833	84.4860	84.4868	83.7512
25	4d <sup>8</sup> 4f	3/2	682437	4d <sub>4/2</sub> <sup>4</sup> f <sub>5/2</sub>	84.4992	84.6114	84.7406	84.8364
26	4d <sup>8</sup> 5p	5/2	682838	(4d <sub>3/2</sub> <sup>3</sup> 4d <sub>5/2</sub> <sup>5</sup> ) <sub>2</sub> 5p <sub>3/2</sub>	84.7124	84.6612	84.6886	83.9971
27	4d <sup>8</sup> 5p	3/2	682998	(4d <sub>3/2</sub> <sup>3</sup> 4d <sub>5/2</sub> <sup>5</sup> ) <sub>3</sub> 5p <sub>3/2</sub>	84.8127	84.6810	84.6763	84.1210
28	4d <sup>8</sup> 5p	7/2	684240	(4d <sub>3/2</sub> <sup>3</sup> 4d <sub>5/2</sub> <sup>5</sup> ) <sub>2</sub> 5p <sub>3/2</sub>	84.8282	84.8350	84.8315	84.2146
29	4d <sup>8</sup> 4f	1/2	684807	4d <sub>4/2</sub> <sup>4</sup> f <sub>7/2</sub>	84.7890	84.9053	84.9555	84.9699
30	4d <sup>8</sup> 4f	7/2	687770	4d <sub>4/2</sub> <sup>4</sup> f <sub>7/2</sub>	85.1100	85.2727	85.2648	85.3875
31	4d <sup>8</sup> 5p	3/2	688121	4d <sub>2/2</sub> <sup>5</sup> p <sub>3/2</sub>	85.5122	85.3162	85.3159	84.7514
32	4d <sup>8</sup> 4f	3/2	689190	4d <sub>4/2</sub> <sup>4</sup> f <sub>5/2</sub>	85.2771	85.4487	85.4144	85.6617
33	4d <sup>8</sup> 5p	5/2	690757	(4d <sub>3/2</sub> <sup>3</sup> 4d <sub>5/2</sub> <sup>5</sup> ) <sub>4</sub> 5p <sub>3/2</sub>	85.6074	85.6430	85.6177	84.9183
34	4d <sup>8</sup> 5p	5/2	694056	(4d <sub>3/2</sub> <sup>3</sup> 4d <sub>5/2</sub> <sup>5</sup> ) <sub>1</sub> 5p <sub>3/2</sub>	86.2761	86.0520	86.0376	85.5415
35	4d <sup>8</sup> 5p	1/2	695239	(4d <sub>3/2</sub> <sup>3</sup> 4d <sub>5/2</sub> <sup>5</sup> ) <sub>1</sub> 5p <sub>3/2</sub>	86.5389	86.1987	86.4222	85.8222
36	4d <sup>8</sup> 4f	3/2	697440	4d <sub>4/2</sub> <sup>4</sup> f <sub>7/2</sub>	86.3697	86.4716	86.5023	86.7867
37	4d <sup>8</sup> 4f	5/2	698751	(4d <sub>3/2</sub> <sup>3</sup> 4d <sub>5/2</sub> <sup>5</sup> ) <sub>2</sub> 4f <sub>5/2</sub>	86.8275	86.6341	86.6812	86.9352
38	4d <sup>8</sup> 4f	5/2	701155	(4d <sub>3/2</sub> <sup>3</sup> 4d <sub>5/2</sub> <sup>5</sup> ) <sub>3</sub> 4f <sub>7/2</sub>	86.5695	86.9322	86.9251	87.1944
39	4d <sup>8</sup> 5p	5/2	701735	4d <sub>2/2</sub> <sup>5</sup> p <sub>3/2</sub>	87.1092	87.0041	87.0408	86.3731
40	4d <sup>8</sup> 4f	1/2	702652	(4d <sub>3/2</sub> <sup>3</sup> 4d <sub>5/2</sub> <sup>5</sup> ) <sub>3</sub> 4f <sub>7/2</sub>	86.9067	87.1178	87.1082	87.2971
41	4d <sup>8</sup> 5p	7/2	703997	(4d <sub>3/2</sub> <sup>3</sup> 4d <sub>5/2</sub> <sup>5</sup> ) <sub>4</sub> 5p <sub>3/2</sub>	87.5382*	87.2845	87.2566	86.8773
42	4d <sup>8</sup> 5p	1/2	705669	(4d <sub>3/2</sub> <sup>3</sup> 4d <sub>5/2</sub> <sup>5</sup> ) <sub>2</sub> 5p <sub>3/2</sub>	87.7952	87.4918	87.4907	87.0046
43	4d <sup>8</sup> 4f	7/2	708748	4d <sub>2/2</sub> <sup>5</sup> f <sub>5/2</sub>	87.8852	87.8736	87.8309	88.2534
44	4d <sup>8</sup> 4f	5/2	711392	(4d <sub>3/2</sub> <sup>3</sup> 4d <sub>5/2</sub> <sup>5</sup> ) <sub>4</sub> 4f <sub>7/2</sub>	88.2139	88.2014	88.1999	88.5561
45	4d <sup>8</sup> 4f	5/2	713643	(4d <sub>3/2</sub> <sup>3</sup> 4d <sub>5/2</sub> <sup>5</sup> ) <sub>3</sub> 4f <sub>5/2</sub>	88.4606	88.4805	88.4592	88.9055
46	4d <sup>8</sup> 4f	5/2	721870	4d <sub>2/2</sub> <sup>5</sup> f <sub>7/2</sub>	89.6583	89.5005	89.5035	89.9423
47	4d <sup>8</sup> 5p	1/2	723216	4d <sub>0/2</sub> <sup>5</sup> 5p <sub>1/2</sub>	90.7099	89.6674	89.7097	89.5125
48	4d <sup>8</sup> 4f	1/2	725785	4d <sub>2/2</sub> <sup>4</sup> f <sub>5/2</sub>	90.0249	89.9971	90.0379	90.3918
49	4d <sup>8</sup> 4f	1/2	737104	4d <sub>2/2</sub> <sup>4</sup> f <sub>5/2</sub>	91.8734	91.3893	91.4296	91.9682

**Table 4.** Cont.

Index	Configuration	J	Level <sup>†</sup>	State	Present	Exp [5]	HFR [15]	MCDHF [15]
50	4d <sup>8</sup> 5p	3/2	745212	$4d_0^2 5p_{3/2}$	92.9879	92.3946	92.3705	92.0573
51	4d <sup>8</sup> 4f	3/2	749681	$(4d_{3/2}^3 4d_{5/2}^5)_2 4f_{5/2}$	90.9563 *	92.9486	92.8513	93.7464
52	4d <sup>8</sup> 4f	1/2	753489	$(4d_{3/2}^3 4d_{5/2}^5)_2 4f_{5/2}$	94.3872	93.4208	93.4519	94.4965
53	4d <sup>8</sup> 4f	5/2	864592	$4d_4^4 4f_{7/2}$	106.0721 *	107.1958	107.1838	109.8049
54	4d <sup>8</sup> 4f	7/2	870470	$4d_2^4 4f_{7/2}$	107.4877 *	107.9246	108.0401	110.2660
55	4d <sup>8</sup> 4f	3/2	874794	$4d_2^2 4f_{5/2}$	107.6293 *	108.4607	108.4489	110.8660
56	4d <sup>8</sup> 4f	5/2	887203	$4d_2^2 4f_{5/2}$	109.4709 *	109.9992	110.0328	112.3180
57	4p <sup>5</sup> 4d <sup>10</sup>	1/2	924721	$4p_{1/2}$	116.2848 *	114.6508	114.6494	115.8723

<sup>†</sup> Energy levels (in cm<sup>-1</sup>) as represented in Churilov and Joshi [5]. \* Values with 4d<sup>6</sup>4f<sup>3</sup> configuration included.

**Table 5.** Same as Table 2 but for Xe<sup>10+</sup>.

Index	Configuration	J	Level <sup>†</sup>	State	Present	Exp [6]	HFR [14]	RCI [14]
1	4d <sup>8</sup>	4	0	$4d_4^4$	0.0000	0.0000	0.0000	0.0000
2	4d <sup>8</sup>	2	13140	$4d_2^4$	1.7415	1.6292	1.6811	1.8015
3	4d <sup>8</sup>	3	15205	$4d_{3/2}^3 4d_{5/2}^5$	1.8204	1.8852	1.8617	1.8688
4	4d <sup>8</sup>	2	26670	$4d_{3/2}^3 4d_{5/2}^5$	3.4080	3.3067	3.3112	3.4620
5	4d <sup>8</sup>	0	32210	$4d_0^4$	4.2453	3.9935	4.0264	2.5905
6	4d <sup>8</sup>	1	34610	$4d_{3/2}^3 4d_{5/2}^5$	4.5407	4.2911	4.3065	4.5968
7	4d <sup>8</sup>	4	40835	$4d_{3/2}^3 4d_{5/2}^5$	5.4872	5.0629	5.0460	5.3922
8	4d <sup>8</sup>	2	42900	$4d_2^2$	5.4003	5.3189	5.3556	5.5356
9	4d <sup>8</sup>	0	88130	$4d_0^2$	11.0871	10.9267	10.9460	9.7872
10	4d <sup>7</sup> 5p	3	725825	$(4d_{3/2}^3 4d_4^4)_{5/2} 5p_{1/2}$	89.8310	89.9909	90.0196	89.8633
11	4d <sup>7</sup> 5p	4	731458	$(4d_{3/2}^3 4d_4^4)_{7/2} 5p_{3/2}$	90.4439	90.6893	90.7270	90.5293
12	4d <sup>7</sup> 5p	3	733755	$4d_{9/2}^3 5p_{3/2}$	90.7887	90.9741	91.0248	90.8299
13	4d <sup>7</sup> 5p	4	737388	$(4d_{3/2}^3 4d_4^4)_{7/2} 5p_{3/2}$	91.1980	91.4245	91.4241	91.1814
14	4d <sup>7</sup> 5p	4	739542	$(4d_{3/2}^3 4d_2^4)_{7/2} 5p_{1/2}$	91.5316	91.6916	91.7102	91.6168
15	4d <sup>7</sup> 5p	5	740348	$(4d_{3/2}^3 4d_4^4)_{11/2} 5p_{1/2}$	91.7221	91.7915	91.7767	91.7197
16	4d <sup>7</sup> 5p	3	741800	$(4d_{3/2}^3 4d_4^4)_{7/2} 5p_{3/2}$	91.8900	91.9715	91.9751	91.8800
17	4d <sup>7</sup> 5p	3	744955	$4d_{3/2}^3 5p_{3/2}$	92.3054	92.3627	92.3530	92.9385
18	4d <sup>7</sup> 5p	1	745470	$(4d_{3/2}^3 4d_2^4)_{3/2} 5p_{1/2}$	92.3464	92.4265	92.4299	92.3399
19	4d <sup>7</sup> 5p	3	749351	$(4d_2^2 4d_5^5)_{5/2} 5p_{1/2}$	92.9282	92.9077	92.9050	93.5021
20	4d <sup>7</sup> 5p	2	750512	$(4d_{3/2}^3 4d_4^4)_{7/2} 5p_{3/2}$	93.1118	93.0517	93.0693	93.4798
21	4d <sup>7</sup> 5p	2	753795	$(4d_{3/2}^3 4d_2^4)_{1/2} 5p_{3/2}$	93.4853	93.4587	93.4608	93.8036
22	4d <sup>7</sup> 5p	1	754745	$4d_{3/2}^3 5p_{3/2}$	93.8957	93.5765	93.6211	93.7532
23	4d <sup>7</sup> 5p	4	756016	$(4d_2^2 4d_5^5)_{9/2} 5p_{1/2}$	93.6887	93.7341	93.7260	93.7626
24	4d <sup>7</sup> 5p	1	758337	$(4d_{3/2}^3 4d_4^4)_{5/2} 5p_{3/2}$	94.4733	94.0218	94.0413	94.2022
25	4d <sup>7</sup> 5p	3	761266	$(4d_{3/2}^3 4d_4^4)_{5/2} 5p_{3/2}$	94.3337	94.3850	94.3938	95.3887
26	4d <sup>7</sup> 5p	4	763070	$(4d_{3/2}^3 4d_2^4)_{7/2} 5p_{3/2}$	94.5816	94.6087	94.6466	94.6785
27	4d <sup>7</sup> 5p	1	765770	$(4d_{3/2}^3 4d_2^4)_{1/2} 5p_{3/2}$	95.2934	94.9434	94.9681	95.4116
28	4d <sup>7</sup> 5p	3	766860	$(4d_{3/2}^3 4d_2^4)_{7/2} 5p_{3/2}$	95.0988	95.0786	95.0791	96.0978
29	4d <sup>7</sup> 5p	1	767369	$(4d_{3/2}^3 4d_2^4)_{3/2} 5p_{3/2}$	95.2028	95.1417	95.1611	95.1833
30	4d <sup>7</sup> 5p	2	773315	$(4d_2^2 4d_5^5)_{3/2} 5p_{3/2}$	96.1325	95.8789	95.9466	96.4209
31	4d <sup>7</sup> 5p	3	773715	$(4d_2^2 4d_5^5)_{7/2} 5p_{3/2}$	96.1320	95.9285	95.9088	96.9597

**Table 5.** Cont.

Index	Configuration	J	Level <sup>†</sup>	State	Present	Exp [6]	HFR [14]	RCI [14]
32	4d <sup>7</sup> 5p	4	773968	(4d <sub>3/2</sub> <sup>2</sup> 4d <sub>4</sub> <sup>4</sup> ) <sub>11/2</sub> <sup>5</sup> p <sub>3/2</sub>	96.3462	95.9598	95.9886	96.3065
33	4d <sup>7</sup> 5p	1	775030	(4d <sub>2</sub> <sup>2</sup> 4d <sub>5/2</sub> <sup>5</sup> ) <sub>3/2</sub> <sup>5</sup> p <sub>3/2</sub>	96.4126	96.0915	96.1071	96.2977
34	4d <sup>7</sup> 5p	3	780503	(4d <sub>2</sub> <sup>2</sup> 4d <sub>5/2</sub> <sup>5</sup> ) <sub>9/2</sub> <sup>5</sup> p <sub>3/2</sub>	97.1319	96.7701	96.8204	97.9562
35	4d <sup>7</sup> 5p	1	784035	(4d <sub>2</sub> <sup>2</sup> 4d <sub>5/2</sub> <sup>5</sup> ) <sub>1/2</sub> <sup>5</sup> p <sub>3/2</sub>	97.4966	97.2080	97.2402	97.4814
36	4d <sup>7</sup> 5p	2	786580	4d <sub>3/2</sub> <sup>5</sup> p <sub>3/2</sub>	97.6818	97.5235	97.5240	97.4868
37	4d <sup>7</sup> 5p	5	789029	(4d <sub>2</sub> <sup>2</sup> 4d <sub>5/2</sub> <sup>5</sup> ) <sub>9/2</sub> <sup>5</sup> p <sub>3/2</sub>	97.9360	97.8272	97.8676	97.9756
38	4d <sup>7</sup> 5p	1	791805	4d <sub>3/2</sub> <sup>5</sup> p <sub>3/2</sub>	98.5246	98.1714	98.1737	100.6760
39	4d <sup>7</sup> 5p	3	795135	4d <sub>3/2</sub> <sup>5</sup> p <sub>3/2</sub>	98.9541	98.5842	98.5785	99.8198
40	4d <sup>7</sup> 5p	3	801225	(4d <sub>0</sub> <sup>2</sup> 4d <sub>5/2</sub> <sup>5</sup> ) <sub>5/2</sub> <sup>5</sup> p <sub>1/2</sub>	99.9998	99.3393	99.3609	100.7918
41	4d <sup>7</sup> 5p	1	830260	(4d <sub>0</sub> <sup>2</sup> 4d <sub>5/2</sub> <sup>5</sup> ) <sub>5/2</sub> <sup>5</sup> p <sub>3/2</sub>	103.9132	102.9392	103.0239	103.4795
42	4d <sup>7</sup> 4f	4	892420	4d <sub>3/2</sub> <sup>3</sup> 4f <sub>7/2</sub>	110.8675	110.6460	110.6962	113.0177
43	4d <sup>7</sup> 4f	3	894941	(4d <sub>3/2</sub> <sup>3</sup> 4d <sub>4</sub> <sup>4</sup> ) <sub>11/2</sub> <sup>4</sup> f <sub>5/2</sub>	111.3093	110.9586	111.0141	113.5215
44	4d <sup>7</sup> 4f	5	897383	4d <sub>9/2</sub> <sup>3</sup> 4f <sub>7/2</sub>	110.9844	111.2614	111.2278	113.2369
45	4d <sup>7</sup> 4f	3	908390	4d <sub>3/2</sub> <sup>3</sup> 4f <sub>7/2</sub>	112.8340	112.6261	112.6093	114.9623
46	4d <sup>7</sup> 4f	4	911082	(4d <sub>2</sub> <sup>2</sup> 4d <sub>5/2</sub> <sup>5</sup> ) <sub>5/2</sub> <sup>4</sup> f <sub>5/2</sub>	112.7247	112.9598	112.9980	115.0362
47	4d <sup>7</sup> 4f	2	911665	(4d <sub>2</sub> <sup>2</sup> 4d <sub>5/2</sub> <sup>5</sup> ) <sub>9/2</sub> <sup>4</sup> f <sub>5/2</sub>	112.7447	113.0321	113.0446	115.4546
48	4d <sup>7</sup> 4f	3	912600	(4d <sub>3/2</sub> <sup>3</sup> 4d <sub>4</sub> <sup>4</sup> ) <sub>7/2</sub> <sup>4</sup> f <sub>7/2</sub>	113.3634	113.1480	113.1855	115.4796
49	4d <sup>7</sup> 4f	1	913877	(4d <sub>3/2</sub> <sup>3</sup> 4d <sub>4</sub> <sup>4</sup> ) <sub>7/2</sub> <sup>4</sup> f <sub>7/2</sub>	112.8179	113.3064	113.3154	116.2031
50	4d <sup>7</sup> 4f	2	924500	(4d <sub>3/2</sub> <sup>3</sup> 4d <sub>4</sub> <sup>4</sup> ) <sub>5/2</sub> <sup>4</sup> f <sub>7/2</sub>	113.9633	114.6234	114.6270	117.0618
51	4d <sup>7</sup> 4f	4	925626	(4d <sub>3/2</sub> <sup>3</sup> 4d <sub>4</sub> <sup>4</sup> ) <sub>11/2</sub> <sup>4</sup> f <sub>7/2</sub>	114.0579	114.7631	114.7761	117.6640
52	4d <sup>7</sup> 4f	0	933343	(4d <sub>2</sub> <sup>2</sup> 4d <sub>5/2</sub> <sup>5</sup> ) <sub>5/2</sub> <sup>4</sup> f <sub>5/2</sub>	117.7646	115.7198	115.7151	118.1618
53	4d <sup>7</sup> 4f	3	935035	4d <sub>3/2</sub> <sup>4</sup> f <sub>5/2</sub>	115.4998	115.9296	115.9595	118.3774
54	4d <sup>7</sup> 4f	5	938628	(4d <sub>2</sub> <sup>2</sup> 4d <sub>5/2</sub> <sup>5</sup> ) <sub>9/2</sub> <sup>4</sup> f <sub>5/2</sub>	116.8915	116.3751	116.4192	118.7650
55	4p <sup>5</sup> 4d <sup>9</sup>	2	944705	4p <sub>1/2</sub> <sup>4</sup> d <sub>3/2</sub> <sup>3</sup>	118.9159	117.1285	117.1295	119.3615
56	4p <sup>5</sup> 4d <sup>9</sup>	2	951795	4p <sub>1/2</sub> <sup>4</sup> d <sub>5/2</sub> <sup>5</sup>	120.5650	118.0076	118.0396	120.3551
57	4p <sup>5</sup> 4d <sup>9</sup>	3	957488	4p <sub>1/2</sub> <sup>4</sup> d <sub>5/2</sub> <sup>5</sup>	122.7719	118.7134	118.7241	121.5465

<sup>†</sup> Energy levels (in cm<sup>-1</sup>) as represented in Churilov et al. [6].

Table 2 presents a comparison of our results for Xe<sup>7+</sup> with the NIST values [23]. In addition to the  $j - j$  coupling representation, we have also included the notations of the states used in the NIST database to make the comparison convenient between the two sets of the results. We find from Table 2 that our calculated energies show an average deviation of nearly 1.5% with the corresponding energies from the NIST database [23]. A maximum variation of nearly 3% is found for the 5s4f  $^3P_{1/2,3/2}$  levels. We have listed only those levels in Table 2 that are reported to be involved in emitting intense lines in the EBIT measurements of Fahy et al. [8] and Ali and Nakamura [9].

For Xe<sup>8+</sup>, in our calculations we got two levels with leading contribution from 4d<sup>9</sup>7p  $^1P_1$ , one at 138.7018 eV (53.65% 4d<sub>5/2</sub><sup>5</sup>7p<sub>3/2</sub>  $^1P + 37.44\% 4d_{3/2}^3 7\bar{p}_{1/2} \ ^3P + 8.79\% 4d_{3/2}^3 7p_{3/2} \ ^3D$ ) and another at 140.2617 eV (44.29% 4d<sub>5/2</sub><sup>5</sup>7p<sub>3/2</sub>  $^1P + 30.70\% 4d_{3/2}^3 7\bar{p}_{1/2} \ ^3P + 24.90\% 4d_{3/2}^3 7p_{3/2} \ ^3D$ ). Considering the maximum contribution, we have classified the level at 138.7018 eV as 4d<sup>9</sup>7p  $^1P_1$ , and 140.2617 eV as 4d<sup>9</sup>7p  $^3P_1$ . This changed the energy order of  $^1P_1$  and  $^3P_1$  in our calculations with respect to those reported by Churilov and Joshi [5]. As can be seen from Table 3, the agreement between the measurements [5] and our results is within 0.8% for most of the cases. The maximum difference of nearly 3 eV is found for the 4d<sup>9</sup>4f  $^1P_1$  level.

The energy levels of Xe<sup>9+</sup> are listed in Table 4 and are compared with the measurements [5] as well as HFR and MCDHF calculations of Motoumba et al. [15]. The open-shell structure of Xe<sup>9+</sup> leads to the formation of a large number of closely spaced fine-structure

levels for its ground and excited state configurations. Consequently, it becomes extremely difficult to correctly identify these states as well as to label them uniquely in LS coupling notations. Churilov and Joshi [5] reported  $\text{Xe}^{9+}$  levels with the wavenumbers (in  $\text{cm}^{-1}$ ) which are also included in Table 4 to guide us in right recognition of the states. From our calculations, we found that the inclusion of the triple excitation  $4\text{d}^64\text{f}^3$  improves the match between the present energies and measurements for the higher  $4\text{d}^84\text{f}$  levels, while it deteriorates the agreement for other levels. Thus we have considered two sets of calculations for  $\text{Xe}^{9+}$ , one with and the other without including the CSF  $4\text{d}^64\text{f}^3$ . The energies marked with \* in Table 4 indicate the inclusion of the CSF  $4\text{d}^64\text{f}^3$ . For  $4\text{p}^54\text{d}^{10}$  levels, our energy results overestimate the measurements [5] and theoretical results [15] by nearly 2 eV. Except for this transition, in most of the cases our energies show better agreements with the experimental results than the MCDHF calculations [15].

Table 5 presents a comparison of the present energies with the experimental energies from Churilov et al. [6] and RCI and HFR calculations of Motoumba et al. [14] for  $\text{Xe}^{10+}$ . Similar to  $\text{Xe}^{9+}$ ,  $\text{Xe}^{10+}$  has an open shell structure and hence, we have included the wavenumbers reported in [6] so that the small spaced levels can be rightly identified. We learnt that adding the CSF  $4\text{p}^44\text{d}^{10}$  improves the energy of the  $4\text{d}^8$  levels, while including the CSF  $4\text{d}^54\text{f}^3$  with triple excitation improves the energy of the higher  $4\text{d}^74\text{f}$  levels. The order of a few levels from  $4\text{d}^8$ ,  $4\text{d}^75\text{p}$  and  $4\text{d}^74\text{f}$  configurations are not as per the order reported in the measurements [6]. Similar cases are also observed in the RCI results [14]. Our reported energies show a deviation of nearly 2–4 eV for the  $4\text{p}^54\text{d}^9$  levels, however, they are in good agreement with the RCI calculations by Motoumba et al. [14].

The comparison of our calculated wavelengths and transition rates with other theoretical and experimental results is shown through Tables 6–9. For  $\text{Xe}^{7+}$ , Table 6 includes the measurements from NIST EBIT and Cowan code calculations reported by Fahy et al. [8], compact EBIT results from Ali and Nakamura [9] as well as HFR calculations of Churilov and Joshi [5]. Though Table 6 shows a maximum deviation of 3.5 Å for levels of  $4\text{d}^95\text{s}4\text{f}$  configurations with indices 9 and 10, a good agreement is found between our reported transition rates and the calculated results from Cowan code [8].

Wavelengths and transition rates for  $\text{Xe}^{8+}$  from the present work are reported and compared in Table 7 with the measurements and other calculations [5,8–10,13]. Overall, our calculations are in good agreement with other results. However, a maximum deviation of 3.4 Å is found in the wavelength corresponding to  $1 \rightarrow 15$  ( $4\text{d}^{10} \ ^1\text{S}_0 \rightarrow 4\text{d}^94\text{f} \ ^1\text{P}_1$ ) transition. This is because from Table 3 our calculated energy of the  $4\text{d}^94\text{f} \ ^1\text{P}_1$  level is overestimated by nearly 3 eV in comparison to the result reported by Churilov and Joshi [5]. It is further noticed for the above transition that our calculated wavelength shows a better match with that from Ivanova [13] and there is a good agreement among various values of the transition rate.

**Table 6.** Wavelengths and transition rates of  $\text{Xe}^{7+}$  for the transitions from  $4\text{d}^{10}5\text{s} \ ^2\text{S}_{1/2}$  state.

Index	$J_b$	Wavelength (nm)		Transition Rate (A) ( $10^{10}$ ) ( $\text{s}^{-1}$ )	
		Present	Other Reported	Present	Other Reported
10	3/2	11.9593	12.32 <sup>a</sup> , 12.56 <sup>b</sup> , 12.332 <sup>c</sup> , 12.3243 <sup>d</sup>	128.093	140.75 <sup>b</sup> , 211.225 <sup>d</sup>
9	1/2	11.9713	12.56 <sup>b</sup> , 12.3265 <sup>d</sup>	122.349	141 <sup>b</sup> , 210.8 <sup>d</sup>
8	1/2	16.5963	16.668 <sup>c</sup>	1.934	
7	3/2	17.0015	17.09 <sup>a</sup> , 17.09 <sup>b</sup> , 17.087 <sup>c</sup>	3.131	4 <sup>b</sup>
6	1/2	17.8218	17.6 <sup>a</sup> , 17.61 <sup>b</sup> , 17.603 <sup>c</sup>	0.399	0.35 <sup>b</sup>
5	1/2	17.9319	17.73 <sup>a</sup> , 17.76 <sup>b</sup> , 17.726 <sup>c</sup>	4.740	5 <sup>b</sup>
4	3/2	18.1815	17.98 <sup>a</sup> , 17.92 <sup>b</sup> , 17.958 <sup>c</sup>	0.766	0.5 <sup>b</sup>
3	3/2	18.4659	18.15 <sup>a</sup> , 18.07 <sup>b</sup>	0.050	0.125 <sup>b</sup>
2	3/2	18.7259	18.44 <sup>a</sup> , 18.31 <sup>b</sup> , 18.4322 <sup>c</sup>	0.165	0.25 <sup>b</sup>

Experimental results: <sup>a</sup>—Fahy et al. [8], <sup>c</sup>—Ali and Nakamura [9], <sup>d</sup>—Churilov and Joshi [5]. Theoretical results: <sup>b</sup>—Fahy et al. [8].

**Table 7.** Wavelengths and transition rates of  $\text{Xe}^{8+}$  for the transitions from  $4d^{10} 1S_0$  state.

Index	$J_b$	Wavelength (nm)		Transition Rate (A) ( $10^{-10}$ ) ( $s^{-1}$ )	
		Present	Other Reported	Present	Other Reported
43	1	8.5973	8.5420 <sup>a</sup> , 8.54 <sup>b</sup> , 8.54 <sup>c</sup>	13.099	12.333 <sup>a</sup> , 11.333 <sup>c</sup>
41	1	8.7491	8.6718 <sup>a*</sup>	3.246	3.167 <sup>a</sup>
38	1	8.8106	8.7294 <sup>a*</sup>	0.012	0.033 <sup>a</sup>
35	1	8.8073	8.7190 <sup>a*</sup>	0.110	0.033 <sup>a</sup>
33	1	8.9389	8.7517 <sup>a</sup>	1.783	1.333 <sup>a</sup>
31	1	8.8395	8.8444 <sup>a</sup> , 8.85 <sup>b</sup> , 8.85 <sup>c</sup>	1.686	1.933 <sup>a</sup> , 2.333 <sup>c</sup>
29	1	9.5763	9.6449 <sup>a</sup> , 9.63 <sup>b</sup> , 9.61 <sup>c</sup> , 9.639 <sup>d</sup> , 9.6218 <sup>f</sup>	57.797	51.267 <sup>a</sup> , 46.667 <sup>c</sup>
26	1	9.9908	9.9553 <sup>a</sup> , 9.963 <sup>f</sup>	2.201	2.2 <sup>a</sup>
24	1	10.1195	10.0732 <sup>a*</sup> , 10.0731 <sup>f</sup>	0.114	0.1 <sup>a</sup>
21	1	10.2993	10.2116 <sup>a*</sup>	0.205	0.267 <sup>a</sup>
19	1	10.3791	10.2815 <sup>a</sup> , 10.28 <sup>b</sup> , 10.29 <sup>c</sup> ,	4.599	3.7 <sup>a</sup> , 4 <sup>c</sup>
17	1	10.4826	10.3808 <sup>a</sup> , 10.38 <sup>b</sup> , 10.39 <sup>c</sup> ,	2.878	2.967 <sup>a</sup> , 3 <sup>c</sup>
15	1	11.6265	12.0133 <sup>a</sup> , 12.02 <sup>b</sup> , 12.00 <sup>c</sup> , 12.019 <sup>d</sup> , 11.5787 <sup>f</sup>	157.520	151.8 <sup>a</sup> , 152 <sup>c</sup>
13	1	14.3835	14.3614 <sup>a</sup> , 14.36 <sup>b</sup> , 14.31 <sup>c</sup> , 14.3127 <sup>f</sup>	0.207	0.2 <sup>a</sup> , 0.2 <sup>c</sup>
10	1	15.1469	15.0274 <sup>a</sup> , 15.1155 <sup>f</sup>	0.031	0.033 <sup>a</sup>
7	1	16.2010	16.1742 <sup>a</sup> , 16.18 <sup>b</sup> , 16.15 <sup>c</sup> , 16.177 <sup>e</sup> , 16.1343 <sup>f</sup>	1.700	1.5 <sup>a</sup> , 8.333 <sup>c</sup>
5	1	16.5223	16.5323 <sup>a</sup> , 16.53 <sup>b</sup> , 16.50 <sup>c</sup> , 16.536 <sup>e</sup> , 16.511 <sup>f</sup>	7.129	8.033 <sup>a</sup> , 1.333 <sup>c</sup>
3	1	16.8906	16.8202 <sup>a</sup> , 16.7548 <sup>f</sup>	0.001	0.007 <sup>a</sup>

Experimental results: *a*—Churilov and Joshi [5], *a\**—calculated wavelengths from the energy levels [5], *b*—Fahy et al. [8], *d*—Ali and Nakamura [10], *c*—Ali and Nakamura [9]. Theoretical results: *c*—Fahy et al. [8], *f*—Ivanova [13].

**Table 8.** Wavelengths and transition rates of  $\text{Xe}^{9+}$ . *a* and *b* denote the indices of initial and final levels, respectively.

<i>a</i>	$J_a$	<i>b</i>	$J_b$	Wavelength (nm)				Transition Rate (A) ( $10^{-10}$ ) ( $s^{-1}$ )			
				Present	Exp [5]	HFR [15]	MCDHF [15]	Present	HFR [5]	HFR [15]	MCDHF [15]
2	3/2	57	1/2	10.8507	11.0133	11.0134	10.8926	182.421	189.800	192.000	155.000
1	5/2	56	5/2	11.3258	11.2714	11.2679	11.0387	2.746	1.617	1.717	0.613
1	5/2	55	3/2	11.5196	11.4312	11.4325	11.1833	30.098	123.550	125.500	137.000
2	3/2	56	5/2	11.5388	11.4879	11.4844	11.2437	170.353	177.667	180.000	154.000
1	5/2	54	7/2	11.5347	11.4880	11.4758	11.2441	174.181	180.000	183.750	155.000
1	5/2	53	5/2	11.6887	11.5661	11.5674	11.2913	154.107	163.267	166.333	146.000
2	3/2	55	3/2	11.7400	11.6541	11.6554	11.3938	126.264	47.375	48.250	13.300
1	5/2	51	3/2	13.6312	13.3390	13.3530	13.2255	0.177	0.300	0.199	0.118
1	5/2	50	3/2	13.3334	13.4189	13.4225	13.4682	0.210	0.325	0.393	0.448
2	3/2	52	1/2	13.4232	13.5729	13.5682	13.4112	3.761	3.100	3.390	2.600
2	3/2	50	3/2	13.6297	13.7272	13.7307	13.7747	0.358	0.450	0.365	0.172
1	5/2	46	5/2	13.8285	13.8529	13.8524	13.7849	0.072	0.067	0.082	0.062
2	3/2	49	1/2	13.7987	13.8816	13.8753	13.7883	0.764	1.050	1.210	0.585
1	5/2	45	5/2	14.0158	14.0126	14.0160	13.9456	0.043	0.050	0.041	0.039
2	3/2	48	1/2	14.0885	14.1032	14.0948	14.0344	0.448	0.150	0.019	0.023
1	5/2	43	7/2	14.1075	14.1094	14.1162	14.0487	0.096	0.125	0.166	0.100
2	3/2	47	1/2	13.9797	14.1545	14.1476	14.1754	0.450	0.550	0.635	0.880
1	5/2	41	7/2	14.1635	14.2046	14.2091	14.2712	0.512	0.525	0.514	0.565
1	5/2	39	5/2	14.2332	14.2505	14.2444	14.3545	0.079	0.067	0.059	0.109
1	5/2	36	3/2	14.3551	14.3382	14.3331	14.2861	0.031	0.225	0.104	0.050
2	3/2	45	5/2	14.3435	14.3488	14.3524	14.2745	0.123	0.100	0.127	0.095
2	3/2	44	5/2	14.3846	14.3954	14.3956	14.3322	0.072	0.050	0.026	0.026
1	5/2	34	5/2	14.3706	14.4079	14.4105	14.4941	0.080	0.083	0.073	0.068
1	5/2	33	5/2	14.4829	14.4771	14.4811	14.6004	0.433	0.233	0.230	0.412

Table 8. Cont.

<i>a</i>	<i>J<sub>a</sub></i>	<i>b</i>	<i>J<sub>b</sub></i>	Wavelength (nm)				Transition Rate (A) (10 <sup>10</sup> ) (s <sup>-1</sup> )			
				Present	Exp [5]	HFR [15]	MCDHF [15]	Present	HFR [5]	HFR [15]	MCDHF [15]
1	5/2	32	3/2	14.5390	14.5096	14.5156	14.4737	0.093	0.475	0.455	0.029
2	3/2	42	1/2	14.4548	14.5150	14.5152	14.5939	7.686	10.050	10.350	10.000
1	5/2	31	3/2	14.4990	14.5325	14.5324	14.6292	2.850	2.350	2.338	2.550
1	5/2	30	7/2	14.5675	14.5397	14.5411	14.5202	0.146	0.038	0.049	0.013
2	3/2	40	1/2	14.6061	14.5788	14.5804	14.5438	0.220	0.100	0.065	0.164
2	3/2	39	5/2	14.5713	14.5983	14.5920	14.7032	3.675	3.017	3.150	4.417
2	3/2	38	5/2	14.6643	14.6107	14.6119	14.5614	0.055	0.267	0.380	0.028
1	5/2	28	7/2	14.6159	14.6148	14.6154	14.7224	0.241	0.125	0.141	0.353
1	5/2	27	3/2	14.6186	14.6413	14.6421	14.7388	0.728	0.600	1.003	0.973
1	5/2	26	5/2	14.6359	14.6448	14.6400	14.7605	0.011	0.217	0.243	0.084
1	5/2	25	3/2	14.6728	14.6532	14.6310	14.6145	0.331	0.400	0.181	0.005
2	3/2	37	5/2	14.6197	14.6622	14.6540	14.6059	0.001	0.183	0.207	0.021
2	3/2	35	1/2	14.6696	14.7381	14.7381	14.8026	0.750	0.950	0.910	0.990
1	5/2	23	5/2	14.7713	14.7418	14.7479	14.7139	0.356	0.100	0.105	0.001
1	5/2	21	3/2	14.7334	14.7618	14.7658	14.8638	5.566	5.650	5.925	6.700
2	3/2	34	5/2	14.7154	14.7640	14.7664	14.8497	1.073	1.100	1.093	0.930
1	5/2	20	7/2	14.8033	14.7734	14.7711	14.7386	0.141	0.163	0.155	0.022
1	5/2	19	5/2	14.8043	14.7956	14.8006	14.9278	3.264	5.350	5.750	6.983
1	5/2	18	3/2	14.8358	14.8333	14.8376	14.9588	0.014	1.300	1.238	0.190
2	3/2	33	5/2	14.8331	14.8359	14.8406	14.9613	1.752	2.150	2.183	1.933
2	3/2	32	3/2	14.8920	14.8709	14.8768	14.8283	0.025	1.200	1.163	4.98E-5
2	3/2	31	3/2	14.8500	14.8942	14.8944	14.9915	2.532	3.325	3.675	3.525
1	5/2	16	5/2	14.8871	14.9020	14.8957	15.0272	2.046	2.217	2.450	3.033
1	5/2	15	7/2	14.9443	14.9358	14.9330	15.0673	1.215	2.438	2.413	1.413
1	5/2	14	5/2	14.9971	14.9583	14.9569	15.1121	0.727	1.100	1.145	0.733
2	3/2	29	1/2	14.9798	14.9682	14.9592	14.9520	0.239	0.450	0.250	0.002
2	3/2	27	3/2	14.9755	15.0089	15.0097	15.1067	6.018	6.050	6.775	6.775
2	3/2	26	5/2	14.9937	15.0124	15.0075	15.1295	0.849	0.933	0.990	0.805
2	3/2	25	3/2	15.0324	15.0216	15.0206	14.9761	0.095	0.650	0.081	0.021
2	3/2	24	1/2	15.0536	15.0444	15.0216	15.1750	0.524	0.700	0.880	1.070
1	5/2	13	5/2	15.0447	15.0544	15.0495	15.1753	3.238	3.967	4.067	3.383
1	5/2	12	3/2	15.1143	15.1020	15.1011	15.2491	0.136	0.325	0.323	0.172
2	3/2	23	5/2	15.1358	15.1141	15.1219	15.0805	0.099	0.117	0.074	0.003
2	3/2	22	1/2	15.0778	15.1291	15.1336	15.2218	0.333	0.400	0.414	0.277
2	3/2	21	3/2	15.0960	15.1356	15.1397	15.2380	0.714	0.175	0.158	0.615
1	5/2	11	7/2	15.2049	15.1747	15.1702	15.3278	0.931	1.075	1.118	1.070
2	3/2	19	5/2	15.1705	15.1762	15.1763	15.3053	0.385	0.667	0.743	0.643
1	5/2	10	5/2	15.2245	15.2058	15.2055	15.3540	1.691	1.833	1.867	1.640
2	3/2	16	5/2	15.2574	15.2832	15.2763	15.4098	0.470	0.217	0.228	0.333
1	5/2	8	3/2	15.3249	15.2849	15.2825	15.4489	0.035	0.100	0.098	0.017
2	3/2	13	5/2	15.4230	15.4433	15.4381	15.5656	0.225	0.200	0.218	0.253
1	5/2	7	7/2	15.5108	15.4588	15.4604	15.6294	0.018	0.038	0.038	0.023
1	5/2	6	5/2	15.5055	15.4680	15.4682	15.6368	0.252	0.317	0.342	0.275
2	3/2	12	3/2	15.4962	15.4935	15.4924	15.6432	0.344	0.325	0.353	0.305
1	5/2	5	3/2	15.5325	15.5248	15.5287	15.4661	0.043	0.050	0.039	0.495
2	3/2	9	1/2	15.6492	15.6300	15.6327	15.7993	0.004	0.050	0.036	0.013
2	3/2	8	3/2	15.7176	15.6857	15.6833	15.8536	0.009	0.050	0.045	0.037
1	5/2	4	3/2	15.4108	15.8924	15.8973	15.6936	0.253	0.300	0.535	0.041
1	5/2	3	7/2	15.9560	15.8972	15.8947	16.0914	0.012	0.025	0.020	0.015
2	3/2	5	3/2	15.9361	15.9388	15.9428	15.8717	0.182	0.125	0.155	0.008
2	3/2	4	3/2	15.8079	16.3262	16.3316	16.1114	0.004	0.050	0.061	0.148

**Table 9.** Wavelengths and transition rates of  $\text{Xe}^{10+}$ .  $a$  and  $b$  refer to the indices of initial and final levels, respectively.

$a$	$J_a$	$b$	$J_b$	Wavelength (nm)			Transition Rate (A) ( $10^{10}$ ) ( $\text{s}^{-1}$ )				
				Present	Exp [6]	HFR [14]	RCI [14]	Present	HFR [6]	HFR [14]	RCI [14]
3	3	57	3	10.2507	10.6125	10.6094	10.3598	9.089	14.486	14.286	10.286
6	1	56	2	10.6861	10.9027	10.9013	10.7106	83.644	60.560	61.000	52.200
7	4	57	3	10.5712	10.9093	10.9066	10.6741	173.558	151.143	152.857	128.000
8	2	57	3	10.5634	10.9339	10.9364	10.6873	13.424	19.071	19.429	16.714
8	2	56	2	10.7658	11.0026	11.0028	10.7982	40.687	94.460	95.800	78.400
8	2	55	2	10.9222	11.0889	11.0924	10.8925	141.509	87.940	87.600	74.400
2	2	48	3	11.1075	11.1179	11.1192	10.9066	14.753	28.657	28.143	14.571
6	1	52	0	10.9504	11.1268	11.1288	10.9175	191.711	189.600	191.000	158.000
7	4	54	5	11.1292	11.1384	11.1323	10.9360	191.990	194.364	196.364	165.455
1	4	44	5	11.1713	11.1435	11.1469	10.9491	186.179	189.364	191.818	162.727
3	3	47	2	11.1774	11.1552	11.1514	10.9155	78.606	78.420	84.200	98.000
3	3	46	4	11.1794	11.1622	11.1561	10.9551	182.634	185.556	187.778	161.111
2	2	45	3	11.1605	11.1706	11.1770	10.9565	107.137	147.571	150.000	139.714
1	4	43	3	11.1387	11.1739	11.1684	10.9217	87.638	160.143	161.429	140.571
7	4	53	3	11.2700	11.1834	11.1785	10.9735	0.118	12.786	12.957	11.343
3	3	45	3	11.1684	11.1954	11.1952	10.9630	26.167	22.714	22.286	11.257
1	4	42	4	11.1831	11.2055	11.2004	10.9703	172.910	174.444	176.667	152.222
8	2	53	3	11.2611	11.2089	11.2098	10.9874	92.121	162.857	164.286	142.000
6	1	50	2	11.3308	11.2373	11.2385	11.0243	28.806	41.460	41.800	43.400
7	4	51	4	11.4197	11.3021	11.2990	11.0432	155.527	162.444	16.556	14.778
6	1	49	1	11.4506	11.3731	11.3738	11.1091	66.408	50.433	52.000	38.333
6	1	47	2	11.4584	11.4020	11.4021	11.1841	54.737	27.100	28.800	22.200
7	4	40	3	13.1183	13.1515	13.1458	13.0111	7.707	5.029	5.171	0.054
8	2	40	3	13.1062	13.1865	13.1891	13.0307	1.540	1.771	1.829	0.102
7	4	39	3	13.2651	13.2573	13.2557	13.1301	3.479	7.029	6.886	7.100
4	2	34	3	13.2287	13.2658	13.2590	13.1208	2.749	1.857	1.900	0.002
6	1	36	2	13.3114	13.2983	13.3005	13.3474	2.258	3.380	3.440	1.422
8	2	38	1	13.3138	13.3529	13.0699	12.7538	2.321	4.700	4.700	0.023
7	4	37	5	13.4111	13.3655	13.3573	13.3916	2.955	2.482	2.564	2.864
4	2	30	2	13.3713	13.3934	13.3841	13.3375	4.881	3.920	4.040	0.045
3	3	25	3	13.4018	13.4037	13.3991	13.2575	0.283	4.257	4.300	0.667
1	4	17	3	13.4320	13.4238	13.4250	13.3405	4.862	5.457	5.714	0.071
9	0	41	1	13.3566	13.4750	13.4651	13.2331	6.771	6.733	6.867	5.867
2	2	22	1	13.4540	13.4844	13.4853	13.4836	6.748	4.800	4.867	3.733
8	2	35	1	13.4625	13.4927	13.4935	13.4845	3.525	5.467	5.567	6.767
3	3	23	4	13.4959	13.4987	13.4965	13.4921	5.388	6.456	6.233	3.178
1	4	15	5	13.5174	13.5072	13.5093	13.5177	3.961	5.718	5.736	3.064
4	2	28	3	13.5220	13.5100	13.5106	13.3840	2.332	4.043	3.943	0.281
1	4	14	4	13.5455	13.5219	13.5191	13.5329	1.240	1.178	1.267	0.680
4	2	27	1	13.4934	13.5298	13.5270	13.4839	4.786	4.967	5.133	0.134
3	3	21	2	13.5258	13.5393	13.5355	13.4861	1.369	4.120	4.300	0.980
8	2	34	3	13.5160	13.5571	13.5554	13.4152	1.427	1.614	1.629	1.413
1	4	13	4	13.5951	13.5614	13.5614	13.5975	4.420	3.500	3.556	5.289
3	3	20	2	13.5812	13.5997	13.5936	13.5338	1.859	1.820	1.908	2.380
5	0	29	1	13.6310	13.6025	13.6045	13.3903	2.424	2.500	2.573	1.057
3	3	19	3	13.6085	13.6213	13.6182	13.5305	2.642	3.829	3.986	1.024
1	4	12	3	13.6564	13.6290	13.6209	13.6502	1.642	1.686	1.729	0.766
7	4	32	4	13.6458	13.6401	13.6332	13.6375	6.981	4.122	5.633	1.533
7	4	31	3	13.6780	13.6451	13.6452	13.5402	2.142	2.229	2.371	0.001
2	2	18	1	13.6840	13.6547	13.6624	13.6941	2.273	3.367	3.467	2.187
8	2	33	1	13.6228	13.6584	13.6619	13.6604	1.970	2.867	3.010	2.347
4	2	24	1	13.6149	13.6670	13.6652	13.6636	2.825	3.300	3.137	1.877
1	4	11	4	13.7084	13.6713	13.6656	13.6955	1.087	4.689	4.778	1.756
8	2	31	3	13.6649	13.6829	13.6919	13.5615	2.588	1.914	2.014	1.087
2	2	16	3	13.7533	13.7238	13.7312	13.7640	1.030	2.122	2.200	1.154
1	4	10	3	13.8019	13.7778	13.7730	13.7970	1.203	1.871	1.900	1.186
7	4	26	4	13.9161	13.8459	13.8374	13.8862	0.999	2.214	2.122	1.311

For  $\text{Xe}^{9+}$ , our wavelengths and transition rates are compared with the measurements [5] and HFR and MCDHF results [15] in Table 8. Our reported wavelengths show a good match with the experimental results [5] with an average difference of 0.5 Å. The two transitions  $1 \rightarrow 4$  and  $2 \rightarrow 4$ , where 1, 2 and 4 refer to the indices assigned to the states of  $\text{Xe}^{9+}$ , show a maximum difference of nearly 5 Å. However, their transition rates are in good agreement with the reported results from Churilov and Joshi [5].

In Table 9, measurements and theoretical results from Churilov et al. [6] as well as HFR and RCI results of Motoumba [14] are included for  $\text{Xe}^{10+}$  along with our calculated wavelengths and transition rates. Previous studies [6,24] showed that there are two possible strong transition arrays of  $\text{Xe}^{10+}$  in 11.1 nm–11.3 nm and 13 nm–14 nm regions with possible applications in EUV Lithography [1]. Thus, we have reported results only for the transitions that fall in these ranges for  $\text{Xe}^{10+}$ . The HFR and RCI wavelengths are calculated from the energy levels provided in [14]. Our results show a maximum deviation of nearly 3.5 Å from measurements and HFR calculations. This discrepancy is found for the transitions from the 3rd, 7th and 8th states to the 57th state. Overall, a better match is seen between the present results and the RCI calculations. Our calculated transition rates agree well with the corresponding values from Churilov et al. [6] except for a few cases, that is,  $3 \rightarrow 25$ ,  $3 \rightarrow 21$  and  $1 \rightarrow 11$  transitions. However, the present transition rates are in reasonable agreement with the RCI calculations for these transitions.

### 3.2. Cross Sections and Rate Coefficients

The atomic wavefunctions of the four ions are used in our RDW program to calculate the electron impact excitation cross sections for the E1 transitions in  $\text{Xe}^{7+}$ – $\text{Xe}^{10+}$  ions. In the previous subsection, we have given a detailed comparison of our calculated results for energy levels, wavelengths and transition rates with other experimental and theoretical results and found an overall satisfactory agreement. This ensures the quality of the target ion's wavefunctions that are crucial in determining the accuracy of the scattering parameters. Moreover, the RDW method has been successfully implemented in the previous work on a variety of targets from closed to open-shell systems and neutral atoms to multiply or highly charged ions atoms/ions [25–30]. It has also been found that using RDW cross sections in a collisional radiative (CR) model provides plasma parameters that are in better agreement with the measurements [31–34]. Therefore, the success of a CR model depends heavily on the accuracy of the collision cross sections being fed to the model. In this connection, we have calculated cross sections for 9, 18, 75 and 57 transitions, respectively, for  $\text{Xe}^{7+}$ ,  $\text{Xe}^{8+}$ ,  $\text{Xe}^{9+}$  and  $\text{Xe}^{10+}$ . Their excitation energies, as discussed earlier, lie in the EUV region. For the sake of simplicity in presenting our results, we have shown only a few transitions graphically through Figure 1 for  $\text{Xe}^{8+}$ . However, cross sections for all the transitions considered in the four ions are provided in the supplementary file through Tables S1–S4 in the incident electron energy range 200–3000 eV. We notice the usual behaviour of the cross sections from Figure 1, that is, they decrease with increasing electron energies and their magnitudes follow the increasing order of the transition rates. Transitions which involve the change of the spin of the state have lesser cross sections as compared to those with the same spin.

Further, to make available our cross sections in a convenient manner, we have performed the fitting of our cross sections Equation (4) with two analytical forms. The first form is a rational fit and suitable for low energy, given by:

$$\sigma_{a \rightarrow b} = \frac{\sum_{i=0}^n x_i E^i}{1 + y_1 E + y_2 E^2}, \quad (5)$$

where  $\sigma_{a \rightarrow b}$  is the excitation cross section from the initial level  $a$  to final level  $b$  and  $E$  is the energy of the incident electron. Both the cross section and the energy are considered in atomic units.  $x_i$ s and  $y_i$ s are fitting coefficients. The second fitting, appropriate for high energy, is performed using the Bethe–Born formula, that is,

$$\sigma_{a \rightarrow b} = \frac{1}{E} (d_0 + d_1 \ln(E)). \quad (6)$$

The Bethe–Born fitting is valid for energy above 2000 eV in the present case. The fitting parameters are provided in Tables 10–13 for  $\text{Xe}^{7+}$ ,  $\text{Xe}^{8+}$ ,  $\text{Xe}^{9+}$  and  $\text{Xe}^{10+}$  ions, respectively. The fitted and calculated cross sections agree within 5%.

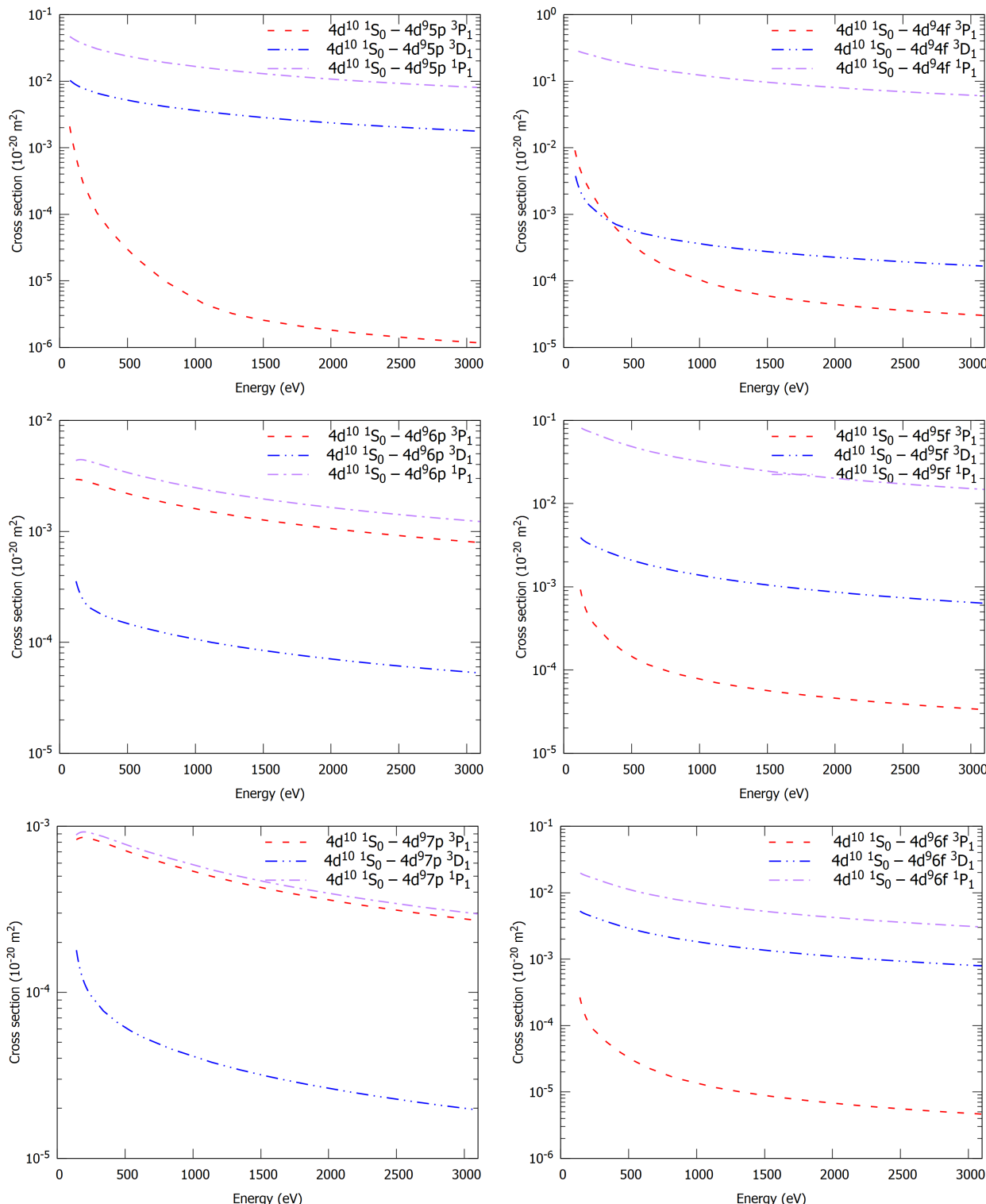


**Figure 1.** Integrated cross sections of  $\text{Xe}^{8+}$  as a function of incident electron energy.

We have also obtained the rate coefficient  $k_{a \rightarrow b}$  at an electron temperature  $T$  for a transition from initial level  $a$  to final level  $b$ . For this purpose, our calculated excitation cross sections are used in the following expression:

$$k_{a \rightarrow b} = 2 \left( \frac{2}{\pi m_e} \right)^{1/2} (k_B T)^{-3/2} \int_{E_{ab}}^{\infty} E \sigma_{a \rightarrow b}(E) \exp \left( -\frac{E}{k_B T} \right) dE, \quad (7)$$

where  $m_e$  represents the mass of electron,  $k_B$  is the Boltzmann constant,  $E_{ab}$  denotes the excitation threshold energy for the transition from  $a$  to  $b$  and  $\sigma_{a \rightarrow b}(E)$  is the calculated cross section at the incident electron energy  $E$ . The rate coefficients are provided through Tables 14–17 for  $\text{Xe}^{7+}$ – $\text{Xe}^{10+}$  ions in the electron temperature range 5–100 eV. The values of rate coefficients rise rapidly at first and then there is a slower logarithmic increase. In order to clearly demonstrate this trend, Figure 2 displays rate coefficients for the transitions reported in Table 7 for  $\text{Xe}^{8+}$ . The same behaviour has been noticed in our previous work on excitation of highly charged xenon ions [25].

**Table 10.** Cross section fitting parameters of  $\text{Xe}^{7+}$  for the transitions from  $4d^{10}5s\ ^2S_{1/2}$  state.

f	$J_f$	$x_0$	$x_1$	$x_2$	$x_3$	$y_1$	$y_2$	$d_0$	$d_1$
10	3/2	5.576E-01	1.286E-02	5.801E-04	-2.658E-06	3.022E-02	3.335E-03	-7.154E+00	4.556E+00
9	1/2	2.882E-01	-3.583E-02	1.310E-05	-	-8.965E-02	-4.299E-03	-3.466E+00	2.192E+00
8	1/2	2.390E-02	3.721E-03	-1.498E-05	1.072E-07	4.181E-01	7.597E-03	-1.399E-01	9.347E-02
7	3/2	6.595E-02	2.499E-03	-2.743E-05	1.472E-07	1.469E-01	1.871E-04	-6.290E-01	3.595E-01
6	1/2	-1.778E-03	-3.447E-03	2.617E-06	-5.192E-08	-1.066E+00	-3.835E-02	-3.549E-02	2.399E-02
5	1/2	6.352E-02	2.428E-03	3.769E-08	-	1.411E-01	1.820E-03	-4.145E-01	2.920E-01
4	3/2	5.399E-02	1.287E-02	-3.358E-05	2.916E-07	1.143E+00	2.860E-02	-1.234E-01	9.544E-02
3	3/2	-4.022E-03	-1.981E-04	1.350E-06	-	-7.126E-01	1.596E-03	-9.671E-03	6.795E-03
2	3/2	-7.036E-03	-1.887E-03	1.368E-05	-8.193E-08	-8.662E-01	-9.805E-03	-1.633E-02	1.929E-02

**Table 11.** Cross section fitting parameters for  $\text{Xe}^{8+}$  for the transitions from  $4d^{10}\ ^1S_0$  state.

f	$J_f$	$x_0$	$x_1$	$x_2$	$x_3$	$y_1$	$y_2$	$d_0$	$d_1$
43	1	1.044E-01	-7.849E-03	-1.655E-05	-	1.709E-02	-7.292E-03	-3.341E-02	7.487E-02
41	1	2.816E-02	-2.014E-03	-4.603E-06	-	2.605E-02	-7.363E-03	-3.341E-02	7.487E-02
38	1	-4.591E-04	2.936E-05	-4.303E-08	6.919E-10	-3.475E-01	1.789E-02	6.634E-04	2.572E-04
35	1	1.021E-04	-9.405E-05	-3.567E-07	8.948E-10	-2.412E-01	-1.337E-02	-3.167E-03	2.348E-03
33	1	6.951E-03	-2.716E-03	-9.772E-06	3.338E-08	-5.202E-01	-2.366E-02	-6.374E-02	3.891E-02
31	1	4.165E-03	-1.042E-03	1.409E-06	-1.362E-08	-2.356E-01	-7.107E-03	-5.827E-02	3.553E-02
29	1	3.780E-01	-2.712E-02	-4.510E-05	-	-6.424E-03	-4.922E-03	-1.935E+00	1.679E+00
26	1	1.775E-02	-4.449E-03	-1.445E-05	-	-1.671E-01	-2.114E-02	-8.387E-02	7.213E-02
24	1	-2.540E-03	2.083E-04	3.607E-06	-1.109E-08	-4.955E-01	3.809E-02	-3.575E-03	3.621E-03
21	1	4.408E-04	-2.197E-04	4.829E-07	-3.464E-09	-2.846E-01	-6.943E-03	-1.061E-02	6.779E-03
19	1	2.079E-02	-5.369E-03	-8.215E-06	-	-2.274E-01	-1.032E-02	-2.413E-01	1.562E-01
17	1	1.443E-02	-5.786E-03	-9.969E-06	-	-3.936E-01	-1.756E-02	-1.552E-01	1.008E-01
15	1	1.214E+00	-4.966E-02	-1.393E-04	-	1.188E-02	-2.411E-03	-1.232E+01	7.758E+00
13	1	-1.350E-02	-6.530E-04	4.946E-06	-1.905E-08	-6.725E-01	-7.720E-04	-2.388E-02	1.930E-02
10	1	-5.999E-02	2.896E-03	-5.797E-05	3.560E-07	-8.149E-01	-1.112E-02	3.911E-03	1.751E-03
7	1	6.010E-02	9.396E-03	-4.047E-05	2.538E-07	4.611E-01	7.450E-03	-3.543E-01	2.263E-01
5	1	2.421E-01	2.923E-02	-5.968E-05	4.494E-07	3.173E-01	6.359E-03	-1.526E+00	1.009E+00
3	1	1.897E-03	1.477E-04	-4.298E-06	3.734E-08	-6.075E-01	1.325E-01	4.609E-04	2.199E-06

**Table 12.** Cross section fitting parameters for  $\text{Xe}^{9+}$ .  $a$  and  $b$  refer to the indices of the initial and final levels, respectively.

a	$J_a$	b	$J_b$	$x_0$	$x_1$	$x_2$	$x_3$	$y_1$	$y_2$	$d_0$	$d_1$
2	3/2	57	1/2	3.056E-01	1.176E-02	-1.971E-05	1.321E-07	1.698E-01	1.873E-03	-1.717E+00	1.207E+00
1	5/2	56	5/2	1.374E-02	1.759E-03	2.290E-06	2.758E-09	4.156E-01	1.212E-02	-5.725E-02	4.089E-02
1	5/2	55	3/2	8.823E-02	6.827E-03	1.098E-05	-5.737E-09	2.423E-01	6.028E-03	-4.267E-01	3.146E-01
2	3/2	56	5/2	1.035E+00	6.391E-02	6.011E-05	1.005E-07	2.016E-01	4.138E-03	-5.513E+00	4.014E+00
1	5/2	54	7/2	9.348E-01	5.812E-02	5.689E-05	8.184E-08	2.015E-01	4.163E-03	-5.017E+00	3.643E+00
1	5/2	53	5/2	6.786E-01	5.081E-02	8.792E-05	-7.732E-08	2.280E-01	5.637E-03	-3.405E+00	2.515E+00
2	3/2	55	3/2	5.657E-01	4.438E-02	8.448E-05	-9.669E-08	2.339E-01	6.025E-03	-2.817E+00	2.086E+00
1	5/2	51	3/2	1.483E-03	-2.150E-03	-6.311E-06	2.082E-08	-4.478E-01	-9.066E-02	7.413E-03	4.252E-03

**Table 12.** Cont.

<i>a</i>	<i>J<sub>a</sub></i>	<i>b</i>	<i>J<sub>b</sub></i>	<i>x<sub>0</sub></i>	<i>x<sub>1</sub></i>	<i>x<sub>2</sub></i>	<i>x<sub>3</sub></i>	<i>y<sub>1</sub></i>	<i>y<sub>2</sub></i>	<i>d<sub>0</sub></i>	<i>d<sub>1</sub></i>
1	5/2	50	3/2	-1.633E-03	-6.857E-04	-1.676E-06	3.357E-09	-8.329E-01	-5.028E-02	-1.824E-03	3.502E-03
2	3/2	52	1/2	-9.315E-03	-1.618E-02	-7.248E-05	1.933E-07	-2.187E+00	-1.254E-01	-6.090E-02	4.506E-02
2	3/2	50	3/2	-8.411E-03	-1.331E-03	-7.320E-07	-3.433E-09	-1.015E+00	-3.252E-02	-6.624E-03	9.189E-03
1	5/2	46	5/2	-9.020E-03	-6.737E-05	-6.880E-06	-	-8.231E-01	-9.125E-02	-1.445E-03	1.805E-03
2	3/2	49	1/2	-6.386E-03	-1.075E-03	-8.103E-06	3.510E-08	-9.694E-01	-4.186E-02	-1.319E-02	9.703E-03
1	5/2	45	5/2	-8.198E-03	2.644E-04	-9.617E-06	6.500E-08	-9.794E-01	-3.430E-02	-5.128E-04	1.133E-03
2	3/2	48	1/2	-4.603E-03	-2.201E-04	4.850E-06	-1.938E-08	-9.938E-01	1.151E-02	-9.463E-03	6.154E-03
1	5/2	43	7/2	-5.336E-03	-3.585E-04	-2.002E-05	1.056E-07	-9.708E-01	-3.847E-01	-1.592E-03	1.153E-03
2	3/2	47	1/2	-7.349E-04	-4.381E-04	-1.050E-07	-1.474E-09	-6.940E-01	-1.885E-02	-9.577E-03	6.063E-03
1	5/2	41	7/2	-2.347E-04	-1.700E-03	-2.480E-06	3.769E-10	-7.088E-01	-2.624E-02	-2.996E-02	1.924E-02
1	5/2	39	5/2	-3.032E-04	-1.082E-04	3.069E-07	-2.097E-09	-5.188E-01	-9.640E-03	-3.506E-03	2.239E-03
1	5/2	36	3/2	-9.068E-03	3.793E-04	-9.565E-06	6.537E-08	-1.031E+00	-1.342E-02	1.092E-03	5.686E-04
2	3/2	45	5/2	-1.961E-02	-6.052E-04	-1.407E-05	-	-1.028E+00	-8.287E-02	-4.095E-03	5.313E-03
2	3/2	44	5/2	4.846E-03	6.598E-04	5.100E-06	-	-3.904E-01	9.545E-02	2.191E-04	2.778E-03
1	5/2	34	5/2	-1.394E-03	-3.671E-04	-3.059E-07	-1.188E-09	-6.339E-01	-3.262E-02	1.056E-05	2.350E-03
1	5/2	33	5/2	-1.103E-03	-1.120E-03	-9.484E-07	-2.286E-09	-7.425E-01	-2.403E-02	-2.029E-02	1.306E-02
1	5/2	32	3/2	-8.471E-03	2.335E-04	-1.088E-05	8.284E-08	-1.071E+00	-2.748E-02	-1.700E-03	1.823E-03
2	3/2	42	1/2	4.540E-02	1.850E-02	-1.009E-05	2.004E-07	1.437E+00	4.170E-02	-1.740E-01	1.142E-01
1	5/2	31	3/2	1.616E-02	-1.804E-03	-2.207E-04	1.562E-06	1.606E-01	-6.303E-02	-8.327E-02	5.704E-02
1	5/2	30	7/2	-3.222E-02	1.096E-03	-3.375E-05	2.293E-07	-1.239E+00	-1.772E-02	-5.527E-03	5.304E-03
2	3/2	40	1/2	-6.778E-03	5.727E-05	-2.581E-06	2.117E-08	-1.105E+00	3.250E-03	-4.217E-03	3.194E-03
2	3/2	39	5/2	1.929E-02	-1.219E-02	-2.534E-05	-	-4.571E-01	-2.306E-02	-2.481E-01	1.680E-01
2	3/2	38	5/2	-1.191E-02	6.834E-05	-5.442E-06	-	-1.034E+00	-3.971E-02	-1.653E-03	2.362E-03
1	5/2	28	7/2	-9.910E-03	-3.222E-04	2.103E-06	-	-1.018E+00	2.659E-03	-1.408E-02	9.679E-03
1	5/2	27	3/2	7.091E-04	-1.521E-03	-4.489E-06	1.017E-08	-7.348E-01	-3.350E-02	-2.288E-02	1.492E-02
1	5/2	26	5/2	-7.491E-04	-2.049E-04	-1.806E-07	-	-5.123E-01	-6.014E-02	1.927E-03	3.460E-04
1	5/2	25	3/2	-1.649E-02	-7.656E-04	-1.481E-05	-	-1.169E+00	-8.421E-02	-9.228E-03	6.756E-03
2	3/2	37	5/2	1.347E-02	-1.652E-04	1.441E-06	-	-1.463E-01	1.037E-01	3.325E-03	-4.932E-04
2	3/2	35	1/2	-6.915E-03	-2.359E-03	-1.747E-06	-3.947E-09	-1.913E+00	-5.451E-02	-1.792E-02	1.170E-02
1	5/2	23	5/2	-2.843E-02	1.988E-04	-1.981E-05	1.415E-07	-1.255E+00	-1.060E-02	-1.509E-02	1.099E-02
1	5/2	21	3/2	3.088E-02	5.424E-03	3.431E-06	-	4.729E-01	1.200E-02	-1.802E-01	1.181E-01
2	3/2	34	5/2	-3.461E-02	-2.093E-02	4.367E-05	-4.088E-07	-3.517E+00	-9.442E-02	-7.586E-02	5.100E-02
1	5/2	20	7/2	1.357E-03	9.443E-04	7.988E-06	-	-4.844E-01	9.045E-02	-4.634E-03	5.359E-03
1	5/2	19	5/2	-7.530E+24	-4.281E+24	-3.989E+21	-	-3.507E+26	-1.152E+25	-1.611E-01	1.053E-01
1	5/2	18	3/2	-4.844E-04	-3.854E-05	-5.814E-09	-	-6.284E-01	-1.850E-02	3.802E-04	3.062E-04
2	3/2	33	5/2	4.114E-04	-1.002E-02	-3.286E-05	8.621E-08	-8.233E-01	-3.897E-02	-1.274E-01	8.530E-02
2	3/2	32	3/2	6.895E-03	8.497E-05	1.816E-06	-	-2.211E-01	1.019E-01	1.099E-03	4.752E-04
2	3/2	31	3/2	8.890E-03	-6.060E-03	-1.281E-05	-	-4.683E-01	-2.365E-02	-1.242E-01	8.251E-02
1	5/2	16	5/2	1.358E-03	-7.669E-03	-2.180E-05	4.608E-08	-8.152E-01	-3.729E-02	-1.020E-01	6.715E-02
1	5/2	15	7/2	-1.196E-03	-7.781E-03	-3.165E-05	9.722E-08	-8.377E-01	-4.796E-02	-6.951E-02	5.389E-02
1	5/2	14	5/2	-1.384E-03	-2.995E-03	-7.747E-06	1.481E-08	-8.195E-01	-3.810E-02	-3.340E-02	2.437E-02
2	3/2	29	1/2	-8.195E-04	-3.932E-04	-6.083E-07	-	-7.390E-01	-2.853E-02	-5.428E-03	3.977E-03
2	3/2	27	3/2	5.091E-02	4.394E-03	-3.825E-05	1.917E-07	3.152E-01	1.431E-03	-3.033E-01	2.013E-01
2	3/2	26	5/2	-1.883E-03	-5.228E-03	-1.323E-05	2.773E-08	-9.040E-01	-3.855E-02	-6.374E-02	4.271E-02
2	3/2	25	3/2	-1.608E-02	4.219E-04	-1.286E-05	8.943E-08	-1.603E+00	-6.194E-03	-3.532E-03	3.001E-03
2	3/2	24	1/2	-2.617E-03	-8.798E-04	1.155E-06	-1.013E-08	-1.011E+00	-2.273E-02	-1.343E-02	8.797E-03
1	5/2	13	5/2	4.754E-03	-1.234E-02	-2.252E-05	-	-7.931E-01	-3.492E-02	-1.657E-01	1.097E-01
1	5/2	12	3/2	-1.464E-03	-5.047E-05	3.431E-06	-1.568E-08	-6.706E-01	1.973E-02	-4.436E-03	3.120E-03
2	3/2	23	5/2	-8.887E-03	3.393E-04	1.236E-05	-4.550E-08	-1.347E+00	7.738E-02	-6.560E-03	4.980E-03
2	3/2	22	1/2	-7.425E-04	-8.053E-04	-2.337E-06	5.950E-09	-1.032E+00	-4.496E-02	-8.145E-03	5.670E-03
2	3/2	21	3/2	-3.277E-03	-3.982E-03	-1.117E-05	2.534E-08	-1.107E+00	-5.097E-02	-3.367E-02	2.447E-02
1	5/2	11	7/2	-2.037E-03	-5.243E-03	-1.403E-05	2.794E-08	-8.092E-01	-3.785E-02	-6.029E-02	4.342E-02
2	3/2	19	5/2	-5.526E-03	-2.375E-03	-8.007E-07	-9.625E-09	-9.796E-01	-3.047E-02	-2.758E-02	2.007E-02
1	5/2	10	5/2	-5.526E-03	-2.375E-03	-8.007E-07	-9.625E-09	-9.796E-01	-3.047E-02	-8.592E-02	5.951E-02
2	3/2	16	5/2	4.399E-04	-3.478E-03	-1.542E-05	4.863E-08	-8.465E-01	-4.849E-02	-3.464E-02	2.494E-02
1	5/2	8	3/2	-6.707E-04	6.903E-05	1.874E-06	-7.268E-09	-6.758E-01	7.029E-02	-1.007E-03	8.332E-04
2	3/2	13	5/2	-7.900E-04	-1.675E-03	-4.275E-06	8.673E-09	-9.697E-01	-4.261E-02	-1.788E-02	1.233E-02
1	5/2	7	7/2	-2.075E-04	1.583E-04	3.899E-06	-1.582E-08	-6.766E-01	1.330E-01	-7.710E-04	8.472E-04
1	5/2	6	5/2	-3.073E-03	-1.153E-03	-7.322E-07	-3.743E-09	-8.339E-01	-3.073E-02	-9.964E-03	9.362E-03
2	3/2	12	3/2	-3.205E-03	-2.176E-03	-5.431E-06	1.109E-08	-1.065E+00	-5.010E-02	-1.519E-02	1.277E-02
1	5/2	5	3/2	-2.835E-03	3.474E-04	4.194E-06	-1.756E-08	-8.477E-01	9.561E-02	1.555E-03	1.078E-03
2	3/2	9	1/2	4.353E-04	2.770E-05	2.759E-07	-	-6.872E-01	2.183E-01	-2.835E-05	6.334E-05
2	3/2	8	3/2	-1.293E-03	4.224E-05	-6.818E-07	3.227E-09	-5.073E-01	1.955E-04	1.282E-05	2.775E-04
1	5/2	4	3/2	-6.739E-02	1.116E-03	-1.703E-05	9.089E-08	-1.792E+00	7.802E-03	2.555E-03	7.192E-03
1	5/2	3	7/2	3.370E-04	3.605E-04	1.689E-06	-	-6.613E-01	1.489E-01	9.439E-04	5.927E-04
2	3/2	5	3/2	-5.758E-04	-1.325E-03	-6.612E-06	2.215E-08	-1.067E+00	-6.396E-02	-9.803E-03	7.328E-03
2	3/2	4	3/2	-3.864E-02	1.479E-03	-2.660E-05	1.627E-07	-1.324E+00	7.284E-03	8.685E-03	6.476E-04

**Table 13.** Cross section fitting parameters for  $\text{Xe}^{10+}$ .  $a$  and  $b$  refer to the indices of the initial and final levels, respectively.

$a$	$J_a$	$b$	$J_b$	$x_0$	$x_1$	$x_2$	$x_3$	$y_1$	$y_2$	$d_0$	$d_1$
3	3	57	3	3.856E−02	3.924E−03	7.081E−06	−6.509E−09	4.070E−01	1.123E−02	−1.383E−01	9.985E−02
6	1	56	2	6.774E−01	7.074E−02	1.372E−04	−1.478E−07	4.034E−01	1.167E−02	−2.190E+00	1.707E+00
7	4	57	3	6.893E−01	6.159E−02	9.215E−05	−3.809E−08	3.926E−01	1.023E−02	−1.975E+00	1.605E+00
8	2	57	3	8.608E−02	8.873E−03	1.555E−05	−1.118E−08	3.964E−01	1.111E−02	−2.862E−01	2.217E−01
8	2	56	2	2.070E−01	2.263E−02	4.735E−05	−6.084E−08	4.225E−01	1.266E−02	−6.544E−01	5.100E−01
8	2	55	2	7.935E−01	9.191E−02	2.120E−04	−3.230E−07	4.528E−01	1.434E−02	−2.329E+00	1.853E+00
2	2	48	3	1.169E−01	1.671E−02	4.725E−05	−9.097E−08	5.033E−01	1.795E−02	−3.641E−01	2.829E−01
6	1	52	0	3.670E−01	4.161E−02	9.169E−05	−1.278E−07	4.516E−01	1.411E−02	−1.045E+00	8.425E−01
7	4	54	5	1.342E+00	1.887E−01	5.396E−04	−1.066E−06	4.967E−01	1.772E−02	−4.146E+00	3.237E+00
1	4	44	5	1.340E+00	1.922E−01	5.601E−04	−1.131E−06	5.109E−01	1.846E−02	−4.056E+00	3.175E+00
3	3	47	2	3.669E−01	4.715E−02	1.266E−04	−2.403E−07	5.117E−01	1.771E−02	−9.723E−01	7.893E−01
3	3	46	4	1.397E+00	1.998E−01	5.833E−04	−1.179E−06	5.124E−01	1.855E−02	−4.192E+00	3.286E+00
2	2	45	3	8.901E−01	1.243E−01	3.531E−04	−6.938E−07	5.056E−01	1.803E−02	−2.655E+00	2.088E+00
1	4	43	3	4.440E−01	5.528E−02	1.411E−04	−2.504E−07	5.055E−01	1.708E−02	−1.162E+00	9.482E−01
7	4	53	3	−7.137E−04	−1.310E−04	−2.108E−07	4.500E−10	−8.434E−01	−2.446E−02	−2.417E−03	1.560E−03
3	3	45	3	1.678E−01	2.262E−02	6.238E−05	−1.203E−07	5.242E−01	1.848E−02	−4.570E−01	3.664E−01
1	4	42	4	1.091E+00	1.469E−01	4.094E−04	−8.016E−07	5.137E−01	1.814E−02	−3.034E+00	2.429E+00
8	2	53	3	8.118E−01	1.212E−01	3.721E−04	−7.946E−07	5.407E−01	2.022E−02	−2.344E+00	1.847E+00
6	1	50	2	3.221E−01	4.756E−02	1.453E−04	−3.097E−07	5.539E−01	2.078E−02	−8.763E−01	7.014E−01
7	4	51	4	1.079E+00	1.696E−01	5.509E−04	−1.248E−06	5.823E−01	2.269E−02	−2.918E+00	2.326E+00
6	1	49	1	4.580E−01	7.460E−02	2.517E−04	−5.931E−07	5.912E−01	2.345E−02	−1.269E+00	1.001E+00
6	1	47	2	6.249E−01	1.035E−01	3.485E−04	−8.087E−07	5.947E−01	2.369E−02	−1.746E+00	1.376E+00
7	4	40	3	−6.599E−02	−6.468E−02	−1.212E−04	8.066E−08	−4.000E+00	−1.507E−01	−2.142E−01	1.338E−01
8	2	40	3	−6.633E−03	−1.035E−02	−1.276E−05	−1.813E−08	−1.862E+00	−6.513E−02	−7.919E−02	4.795E−02
7	4	39	3	−4.284E−02	−3.422E−02	−7.159E−05	8.431E−08	−4.292E+00	−1.691E−01	−9.679E−02	6.300E−02
4	2	34	3	−2.599E−02	−3.106E−02	−5.495E−05	4.580E−08	−3.017E+00	−1.093E−01	−1.452E−01	8.824E−02
6	1	36	2	−7.498E−02	−5.240E−02	−1.229E−04	2.234E−07	−4.902E+00	−1.883E−01	−1.384E−01	8.802E−02
8	2	38	1	−4.106E−03	−5.230E−03	2.451E−06	−5.463E−08	−1.424E+00	−4.290E−02	−5.329E−02	3.259E−02
7	4	37	5	−1.177E−02	−1.583E−02	−1.377E−05	−7.590E−08	−1.439E+00	−5.348E−02	−1.325E−01	8.631E−02
4	2	30	2	−3.874E−02	−4.511E−02	−1.002E−04	1.610E−07	−3.260E+00	−1.246E−01	−1.880E−01	1.155E−01
3	3	25	3	−2.119E−03	−8.258E−04	2.084E−06	−1.516E−08	−1.192E+00	−2.525E−02	−1.124E−02	7.022E−03
1	4	17	3	1.777E+45	1.063E+45	2.215E+42	−	1.010E+47	3.643E+45	−1.483E−01	9.076E−02
9	0	41	1	−1.387E−01	−1.824E−01	−3.238E−04	2.822E−07	−3.300E+00	−1.189E−01	−7.989E−01	4.791E−01
2	2	22	1	−2.337E−02	−3.028E−02	−6.264E−05	8.367E−08	−2.559E+00	−9.786E−02	−1.581E−01	9.771E−02
8	2	35	1	−7.682E−03	−1.075E−02	−1.771E−05	1.329E−08	−1.830E+00	−6.477E−02	−8.502E−02	5.116E−02
3	3	23	4	1.788E+58	1.091E+58	2.091E+55	−	5.632E+59	1.994E+58	−2.775E−01	1.688E−01
1	4	15	5	−2.640E−02	−2.772E−02	−2.200E−05	−9.703E−08	−2.014E+00	−6.763E−02	−1.927E−01	1.188E−01
4	2	28	3	−2.220E−02	−2.563E−02	−4.240E−05	2.213E−08	−2.721E+00	−9.858E−02	−1.307E−01	8.002E−02
1	4	14	4	−5.409E−03	−6.585E−03	−1.025E−05	2.949E−09	−1.821E+00	−6.558E−02	−4.963E−02	3.060E−02
4	2	27	1	−1.486E−02	−1.840E−02	−3.223E−05	1.495E−08	−2.129E+00	−8.117E−02	−1.111E−01	6.996E−02
3	3	21	2	−1.110E−02	−5.965E−03	9.139E−06	−8.721E−08	−2.402E+00	−5.948E−02	−3.898E−02	2.400E−02
8	2	34	3	−6.230E−03	−8.586E−03	−8.745E−06	−2.580E−08	−1.466E+00	−5.191E−02	−7.861E−02	4.892E−02
1	4	13	4	−3.719E−02	−3.551E−02	−7.262E−05	9.392E−08	−2.661E+00	−1.010E−01	−1.755E−01	1.101E−01
3	3	20	2	−4.863E−03	−6.681E−03	−8.585E−06	−7.385E−09	−1.738E+00	−6.104E−02	−5.406E−02	3.297E−02
5	0	29	1	3.633E−02	7.715E−04	−6.337E−06	−	1.444E−01	−5.032E−04	−2.978E−01	1.827E−01
3	3	19	3	−2.710E−02	−2.308E−02	−2.867E−05	−2.763E−08	−3.004E+00	−1.040E−01	−1.065E−01	6.603E−02
1	4	12	3	1.856E−03	−3.206E−03	−1.852E−05	6.647E−08	−6.132E−01	−3.804E−02	−4.826E−02	3.226E−02
7	4	32	4	−4.462E−02	−5.445E−02	−1.052E−04	1.327E−07	−2.618E+00	−9.698E−02	−2.883E−01	1.760E−01
7	4	31	3	−2.038E−02	−1.556E−02	−2.229E−05	−1.144E−08	−3.069E+00	−1.105E−01	−6.650E−02	4.226E−02
2	2	18	1	−8.687E−03	−9.822E−03	−1.700E−05	1.232E−08	−2.372E+00	−8.731E−02	−5.611E−02	3.469E−02
8	2	33	1	−8.895E−03	−7.900E−03	−1.006E−05	−1.118E−08	−2.212E+00	−7.918E−02	−4.668E−02	2.964E−02
4	2	24	1	−1.114E−02	−1.292E−02	−2.677E−05	3.928E−08	−2.530E+00	−9.591E−02	−6.866E−02	4.244E−02
1	4	11	4	−4.827E−03	−4.479E−03	2.534E−07	−4.019E−08	−1.354E+00	−4.395E−02	−4.338E−02	2.779E−02
8	2	31	3	−1.813E−02	−2.261E−02	−2.995E−05	−1.856E−08	−2.118E+00	−7.447E−02	−1.504E−01	9.168E−02
2	2	16	3	−5.591E−03	−5.854E−03	1.359E−06	−5.623E−08	−1.363E+00	−4.263E−02	−5.966E−02	3.723E−02
1	4	10	3	−5.785E−03	−2.121E−03	8.237E−06	−5.687E−08	−1.435E+00	−2.622E−02	−2.446E−02	1.538E−02
7	4	26	4	−4.329E−03	−3.606E−03	5.849E−06	−6.065E−08	−1.192E+00	−3.268E−02	−4.228E−02	2.680E−02

**Table 14.** Rate coefficients for  $\text{Xe}^{7+}$  for the transitions from the state  $4d^{10}5s\ ^2S_{1/2}$  at electron temperatures 5, 10, 20, 30, 50, 70, 100 eV.

Index	$J_f$	5	10	15	20	30	50	70	100
10	3/2	4.754E−23	1.111E−18	2.983E−17	1.507E−16	7.403E−16	2.561E−15	4.301E−15	6.296E−15
9	1/2	2.326E−23	5.378E−19	1.439E−17	7.259E−17	3.560E−16	1.230E−15	2.064E−15	3.020E−15
8	1/2	3.282E−22	4.250E−19	4.351E−18	1.356E−17	4.104E−17	9.603E−17	1.362E−16	1.756E−16
7	3/2	1.548E−21	1.689E−18	1.638E−17	4.981E−17	1.474E−16	3.401E−16	4.805E−16	6.186E−16
6	1/2	2.863E−22	2.176E−19	1.848E−18	5.218E−18	1.419E−17	3.013E−17	4.076E−17	5.054E−17
5	1/2	3.073E−21	2.303E−18	1.974E−17	5.645E−17	1.572E−16	3.456E−16	4.780E−16	6.049E−16
4	3/2	1.513E−21	1.015E−18	8.318E−18	2.315E−17	6.232E−17	1.320E−16	1.787E−16	2.217E−16
3	3/2	4.540E−22	2.561E−19	1.906E−18	4.933E−18	1.184E−17	2.120E−17	2.540E−17	2.758E−17
2	3/2	9.381E−22	4.936E−19	3.642E−18	9.475E−18	2.329E−17	4.412E−17	5.565E−17	6.444E−17

**Table 15.** Rate coefficients for  $\text{Xe}^{8+}$  for the transitions from the state  $4d^{10}\ ^1S_0$  at electron temperatures 5, 10, 20, 30, 50, 70, 100 eV.

Index	$J_b$	5	10	15	20	30	50	70	100
43	1	2.593E−27	3.429E−21	3.495E−19	3.414E−18	3.198E−17	1.807E−16	3.674E−16	6.093E−16
41	1	1.123E−27	1.154E−21	1.082E−19	1.012E−18	9.086E−18	4.956E−17	9.922E−17	1.626E−16
38	1	6.405E−29	5.562E−23	4.740E−21	4.131E−20	3.321E−19	1.547E−18	2.759E−18	3.962E−18
35	1	4.422E−29	3.994E−23	3.516E−21	3.154E−20	2.664E−19	1.345E−18	2.562E−18	4.002E−18
33	1	3.437E−28	2.673E−22	2.309E−20	2.091E−19	1.839E−18	1.011E−17	2.070E−17	3.518E−17
31	1	2.381E−28	2.160E−22	1.962E−20	1.821E−19	1.639E−18	9.172E−18	1.889E−17	3.223E−17
29	1	1.835E−25	5.586E−20	3.501E−18	2.688E−17	1.987E−16	9.355E−16	1.769E−15	2.796E−15
26	1	2.470E−26	4.364E−21	2.275E−19	1.589E−18	1.067E−17	4.629E−17	8.436E−17	1.294E−16
24	1	7.512E−27	1.070E−21	5.033E−20	3.277E−19	1.985E−18	7.497E−18	1.236E−17	1.692E−17
21	1	4.471E−27	5.306E−22	2.387E−20	1.536E−19	9.361E−19	3.693E−18	6.413E−18	9.485E−18
19	1	6.855E−26	7.798E−21	3.552E−19	2.337E−18	1.494E−17	6.366E−17	1.168E−16	1.826E−16
17	1	5.769E−26	5.811E−21	2.537E−19	1.632E−18	1.019E−17	4.252E−17	7.724E−17	1.199E−16
15	1	5.115E−23	1.601E−18	4.726E−17	2.497E−16	1.278E−15	4.531E−15	7.652E−15	1.120E−14
13	1	3.100E−23	1.180E−19	1.668E−18	5.972E−18	1.999E−17	4.738E−17	6.447E−17	7.717E−17
10	1	1.695E−22	4.140E−19	5.012E−18	1.651E−17	5.025E−17	1.071E−16	1.351E−16	1.472E−16
7	1	5.544E−22	8.580E−19	9.307E−18	2.984E−17	9.275E−17	2.215E−16	3.166E−16	4.104E−16
5	1	3.354E−21	4.494E−18	4.655E−17	1.460E−16	4.447E−16	1.046E−15	1.487E−15	1.918E−15
3	1	1.862E−22	1.917E−19	1.715E−18	4.803E−18	1.219E−17	2.161E−17	2.459E−17	2.429E−17

**Table 16.** Rate coefficients for  $\text{Xe}^{9+}$  at electron temperatures 5, 10, 20, 30, 50, 70, 100 eV.  $a$  and  $b$  denote the indices of the initial and final levels, respectively.

$a$	$J_a$	$b$	$J_b$	5	10	15	20	30	50	70	100
2	3/2	57	1/2	2.383E−24	1.587E−19	5.989E−18	3.566E−17	2.043E−16	7.829E−16	1.355E−15	2.002E−15
1	5/2	56	5/2	2.130E−25	8.764E−21	2.815E−19	1.545E−18	8.152E−18	2.922E−17	4.910E−17	7.100E−17
1	5/2	55	3/2	2.345E−24	8.050E−20	2.438E−18	1.301E−17	6.680E−17	2.349E−16	3.918E−16	5.639E−16
2	3/2	56	5/2	2.992E−23	1.010E−18	3.043E−17	1.620E−16	8.309E−16	2.921E−15	4.879E−15	7.033E−15
1	5/2	54	7/2	2.686E−23	9.102E−19	2.746E−17	1.463E−16	7.508E−16	2.642E−15	4.413E−15	6.363E−15
1	5/2	53	5/2	2.498E−23	7.347E−19	2.115E−17	1.100E−16	5.514E−16	1.903E−15	3.152E−15	4.516E−15
2	3/2	55	3/2	2.270E−23	6.375E−19	1.807E−17	9.330E−17	4.640E−16	1.592E−15	2.630E−15	3.762E−15
1	5/2	51	3/2	3.640E−24	2.313E−20	3.949E−19	1.570E−18	5.934E−18	1.595E−17	2.333E−17	2.996E−17
1	5/2	50	3/2	1.068E−24	8.286E−21	1.508E−19	6.185E−19	2.407E−18	6.610E−18	9.761E−18	1.265E−17
2	3/2	52	1/2	6.258E−24	4.673E−20	8.517E−19	3.528E−18	1.409E−17	4.068E−17	6.262E−17	8.526E−17
2	3/2	50	3/2	4.433E−24	2.793E−20	4.728E−19	1.866E−18	6.962E−18	1.836E−17	2.652E−17	3.363E−17
1	5/2	46	5/2	4.080E−24	2.194E−20	3.467E−19	1.308E−18	4.574E−18	1.099E−17	1.473E−17	1.701E−17
2	3/2	49	1/2	4.423E−24	2.486E−20	4.047E−19	1.566E−18	5.731E−18	1.489E−17	2.139E−17	2.703E−17
1	5/2	45	5/2	4.347E−24	2.078E−20	3.161E−19	1.170E−18	4.018E−18	9.509E−18	1.265E−17	1.450E−17
2	3/2	48	1/2	4.152E−24	1.929E−20	2.938E−19	1.097E−18	3.860E−18	9.644E−18	1.354E−17	1.676E−17
1	5/2	43	7/2	2.148E−24	8.938E−21	1.300E−19	4.711E−19	1.588E−18	3.733E−18	4.999E−18	5.834E−18
2	3/2	47	1/2	2.157E−24	1.088E−20	1.717E−19	6.560E−19	2.384E−18	6.244E−18	9.103E−18	1.179E−17
1	5/2	41	7/2	6.800E−24	3.097E−20	4.759E−19	1.803E−18	6.552E−18	1.742E−17	2.581E−17	3.413E−17
1	5/2	39	5/2	1.605E−24	6.755E−21	9.910E−20	3.623E−19	1.244E−18	3.050E−18	4.267E−18	5.303E−18
1	5/2	36	3/2	7.305E−24	2.834E−20	4.022E−19	1.439E−18	4.775E−18	1.099E−17	1.444E−17	1.635E−17
2	3/2	45	5/2	1.533E−23	6.025E−20	8.618E−19	3.103E−18	1.042E−17	2.450E−17	3.286E−17	3.836E−17
2	3/2	44	5/2	2.408E−23	9.221E−20	1.306E−18	4.673E−18	1.555E−17	3.598E−17	4.744E−17	5.394E−17
1	5/2	34	5/2	4.306E−24	1.681E−20	2.411E−19	8.731E−19	2.973E−18	7.226E−18	1.003E−17	1.230E−17

**Table 16.** Cont.

<i>a</i>	<i>J<sub>a</sub></i>	<i>b</i>	<i>J<sub>b</sub></i>	5	10	15	20	30	50	70	100
1	5/2	33	5/2	7.734E−24	2.884E−20	4.129E−19	1.506E−18	5.247E−18	1.338E−17	1.938E−17	2.508E−17
1	5/2	32	3/2	8.124E−24	2.833E−20	3.885E−19	1.368E−18	4.475E−18	1.024E−17	1.350E−17	1.546E−17
2	3/2	42	1/2	4.613E−23	1.794E−19	2.640E−18	9.847E−18	3.555E−17	9.538E−17	1.431E−16	1.921E−16
1	5/2	31	3/2	2.637E−23	9.957E−20	1.449E−18	5.368E−18	1.922E−17	5.112E−17	7.628E−17	1.018E−16
1	5/2	30	7/2	2.690E−23	9.245E−20	1.263E−18	4.442E−18	1.453E−17	3.327E−17	4.382E−17	5.005E−17
2	3/2	40	1/2	8.092E−24	2.731E−20	3.721E−19	1.310E−18	4.313E−18	1.006E−17	1.351E−17	1.587E−17
2	3/2	39	5/2	8.348E−23	3.020E−19	4.332E−18	1.594E−17	5.666E−17	1.498E−16	2.231E−16	2.973E−16
2	3/2	38	5/2	1.412E−23	4.577E−20	6.131E−19	2.134E−18	6.910E−18	1.571E−17	2.066E−17	2.361E−17
1	5/2	28	7/2	1.513E−23	5.111E−20	6.990E−19	2.471E−18	8.200E−18	1.942E−17	2.651E−17	3.191E−17
1	5/2	27	3/2	7.840E−24	2.748E−20	3.892E−19	1.421E−18	5.004E−18	1.310E−17	1.940E−17	2.575E−17
1	5/2	26	5/2	3.487E−24	1.151E−20	1.551E−19	5.417E−19	1.765E−18	4.079E−18	5.473E−18	6.466E−18
1	5/2	25	3/2	1.754E−23	5.701E−20	7.676E−19	2.686E−18	8.794E−18	2.041E−17	2.736E−17	3.212E−17
2	3/2	37	5/2	2.612E−23	8.661E−20	1.166E−18	4.058E−18	1.308E−17	2.922E−17	3.762E−17	4.153E−17
2	3/2	35	1/2	8.531E−24	2.871E−20	3.986E−19	1.435E−18	4.941E−18	1.252E−17	1.808E−17	2.334E−17
1	5/2	23	5/2	3.329E−23	1.023E−19	1.352E−18	4.686E−18	1.519E−17	3.496E−17	4.667E−17	5.457E−17
1	5/2	21	3/2	6.701E−23	2.214E−19	3.085E−18	1.120E−17	3.930E−17	1.031E−16	1.531E−16	2.039E−16
2	3/2	34	5/2	3.199E−23	1.060E−19	1.473E−18	5.324E−18	1.855E−17	4.807E−17	7.077E−17	9.338E−17
1	5/2	20	7/2	4.990E−23	1.496E−19	1.952E−18	6.705E−18	2.141E−17	4.792E−17	6.233E−17	7.021E−17
1	5/2	19	5/2	6.960E−23	2.199E−19	3.011E−18	1.082E−17	3.750E−17	9.691E−17	1.426E−16	1.882E−16
1	5/2	18	3/2	2.000E−24	5.880E−21	7.619E−20	2.608E−19	8.315E−19	1.883E−18	2.500E−18	2.927E−18
2	3/2	33	5/2	6.316E−23	1.953E−19	2.647E−18	9.443E−18	3.243E−17	8.286E−17	1.211E−16	1.588E−16
2	3/2	32	3/2	2.371E−23	6.748E−20	8.645E−19	2.939E−18	9.270E−18	2.045E−17	2.630E−17	2.916E−17
2	3/2	31	3/2	5.716E−23	1.761E−19	2.392E−18	8.560E−18	2.958E−17	7.634E−17	1.124E−16	1.484E−16
1	5/2	16	5/2	5.005E−23	1.504E−19	2.023E−18	7.194E−18	2.466E−17	6.305E−17	9.231E−17	1.213E−16
1	5/2	15	7/2	5.519E−23	1.598E−19	2.115E−18	7.445E−18	2.517E−17	6.324E−17	9.144E−17	1.185E−16
1	5/2	14	5/2	2.637E−23	7.384E−20	9.644E−19	3.368E−18	1.128E−17	2.803E−17	4.028E−17	5.194E−17
2	3/2	29	1/2	5.911E−24	1.642E−20	2.119E−19	7.313E−19	2.397E−18	5.766E−18	8.082E−18	1.012E−17
2	3/2	27	3/2	1.516E−22	4.372E−19	5.824E−18	2.066E−17	7.093E−17	1.827E−16	2.692E−16	3.564E−16
2	3/2	26	5/2	3.923E−23	1.106E−19	1.452E−18	5.093E−18	1.717E−17	4.313E−17	6.249E−17	8.130E−17
2	3/2	25	3/2	1.773E−23	4.711E−20	5.928E−19	2.005E−18	6.334E−18	1.422E−17	1.869E−17	2.147E−17
2	3/2	24	1/2	1.122E−23	3.018E−20	3.867E−19	1.333E−18	4.372E−18	1.056E−17	1.488E−17	1.878E−17
1	5/2	13	5/2	9.271E−23	2.564E−19	3.361E−18	1.182E−17	4.012E−17	1.022E−16	1.496E−16	1.970E−16
1	5/2	12	3/2	9.180E−24	2.314E−20	2.848E−19	9.505E−19	2.958E−18	6.595E−18	8.745E−18	1.032E−17
2	3/2	23	5/2	1.708E−23	4.313E−20	5.355E−19	1.804E−18	5.711E−18	1.302E−17	1.745E−17	2.065E−17
2	3/2	22	1/2	6.343E−24	1.703E−20	2.196E−19	7.625E−19	2.539E−18	6.291E−18	9.032E−18	1.164E−17
2	3/2	21	3/2	2.815E−23	7.500E−20	9.657E−19	3.354E−18	1.118E−17	2.778E−17	3.997E−17	5.162E−17
1	5/2	11	7/2	5.762E−23	1.441E−19	1.813E−18	6.215E−18	2.043E−17	5.007E−17	7.158E−17	9.197E−17
2	3/2	19	5/2	3.113E−23	7.863E−20	9.875E−19	3.371E−18	1.097E−17	2.635E−17	3.707E−17	4.675E−17
1	5/2	10	5/2	6.855E−23	1.713E−19	2.166E−18	7.467E−18	2.480E−17	6.178E−17	8.934E−17	1.162E−16
2	3/2	16	5/2	3.111E−23	7.636E−20	9.594E−19	3.297E−18	1.091E−17	2.709E−17	3.910E−17	5.074E−17
1	5/2	8	3/2	6.708E−24	1.494E−20	1.753E−19	5.679E−19	1.698E−18	3.579E−18	4.538E−18	5.060E−18
2	3/2	13	5/2	1.836E−23	4.113E−20	5.002E−19	1.689E−18	5.481E−18	1.336E−17	1.910E−17	2.461E−17
1	5/2	7	7/2	1.445E−23	2.902E−20	3.275E−19	1.038E−18	3.015E−18	6.128E−18	7.566E−18	8.171E−18
1	5/2	6	5/2	2.825E−23	5.938E−20	6.983E−19	2.301E−18	7.188E−18	1.659E−17	2.279E−17	2.810E−17
2	3/2	12	3/2	2.849E−23	6.095E−20	7.265E−19	2.421E−18	7.711E−18	1.832E−17	2.573E−17	3.246E−17
1	5/2	5	3/2	1.985E−23	3.999E−20	4.555E−19	1.459E−18	4.336E−18	9.195E−18	1.178E−17	1.333E−17
2	3/2	9	1/2	5.039E−24	9.325E−21	1.017E−19	3.152E−19	8.889E−19	1.736E−18	2.079E−18	2.160E−18
2	3/2	8	3/2	1.994E−23	3.579E−20	3.874E−19	1.199E−18	3.385E−18	6.657E−18	8.035E−18	8.436E−18
1	5/2	4	3/2	1.038E−22	2.259E−19	2.666E−18	8.742E−18	2.687E−17	5.941E−17	7.797E−17	8.977E−17
1	5/2	3	7/2	4.994E−23	7.990E−20	8.335E−19	2.534E−18	7.045E−18	1.374E−17	1.659E−17	1.750E−17
2	3/2	5	3/2	1.982E−23	3.436E−20	3.840E−19	1.244E−18	3.873E−18	9.131E−18	1.286E−17	1.635E−17
2	3/2	4	3/2	1.237E−22	2.181E−19	2.388E−18	7.519E−18	2.207E−17	4.647E−17	5.915E−17	6.580E−17

**Table 17.** Rate coefficients for  $\text{Xe}^{10+}$  at electron temperatures 5, 10, 20, 30, 50, 70, 100 eV.  $a$  and  $b$  denote the indices of the initial and final levels, respectively.

$a$	$J_a$	$b$	$J_b$	5	10	15	20	30	50	70	100
3	3	57	3	6.000E−26	7.754E−21	3.640E−19	2.411E−18	1.531E−17	6.323E−17	1.124E−16	1.689E−16
6	1	56	2	2.790E−24	2.205E−19	8.794E−18	5.371E−17	3.146E−16	1.220E−15	2.113E−15	3.114E−15
7	4	57	3	2.171E−24	1.945E−19	8.079E−18	5.035E−17	3.006E−16	1.182E−15	2.056E−15	3.037E−15
8	2	57	3	2.751E−25	2.488E−20	1.038E−18	6.481E−18	3.882E−17	1.532E−16	2.674E−16	3.965E−16
8	2	56	2	9.893E−25	7.177E−20	2.781E−18	1.675E−17	9.668E−17	3.707E−16	6.388E−16	9.381E−16
8	2	55	2	5.066E−24	3.116E−19	1.143E−17	6.695E−17	3.761E−16	1.410E−15	2.407E−15	3.510E−15
2	2	48	3	1.071E−24	5.457E−20	1.881E−18	1.069E−17	5.826E−17	2.137E−16	3.617E−16	5.247E−16
6	1	52	0	2.469E−24	1.475E−19	5.359E−18	3.124E−17	1.746E−16	6.520E−16	1.111E−15	1.617E−15
7	4	54	5	1.287E−23	6.416E−19	2.195E−17	1.243E−16	6.750E−16	2.468E−15	4.173E−15	6.047E−15
1	4	44	5	1.376E−23	6.577E−19	2.219E−17	1.247E−16	6.727E−16	2.446E−15	4.125E−15	5.966E−15
3	3	47	2	3.669E−24	1.742E−19	5.860E−18	3.288E−17	1.769E−16	6.407E−16	1.077E−15	1.553E−15
3	3	46	4	1.452E−23	6.885E−19	2.317E−17	1.300E−16	7.004E−16	2.543E−15	4.287E−15	6.197E−15
2	2	45	3	8.931E−24	4.316E−19	1.461E−17	8.227E−17	4.444E−16	1.617E−15	2.728E−15	3.946E−15
1	4	43	3	4.116E−24	2.030E−19	6.917E−18	3.905E−17	2.114E−16	7.693E−16	1.296E−15	1.871E−15
7	4	53	3	1.136E−26	4.820E−22	1.543E−20	8.382E−20	4.312E−19	1.475E−18	2.386E−18	3.302E−18
3	3	45	3	1.646E−24	7.888E−20	2.662E−18	1.496E−17	8.062E−17	2.926E−16	4.926E−16	7.109E−16
1	4	42	4	1.116E−23	5.272E−19	1.771E−17	9.930E−17	5.340E−16	1.935E−15	3.256E−15	4.699E−15
8	2	53	3	9.624E−24	4.211E−19	1.380E−17	7.640E−17	4.060E−16	1.458E−15	2.447E−15	3.525E−15
6	1	50	2	4.261E−24	1.742E−19	5.579E−18	3.054E−17	1.604E−16	5.707E−16	9.531E−16	1.368E−15
7	4	51	4	1.660E−23	6.233E−19	1.940E−17	1.048E−16	5.426E−16	1.910E−15	3.176E−15	4.544E−15
6	1	49	1	7.470E−24	2.725E−19	8.402E−18	4.515E−17	2.328E−16	8.167E−16	1.357E−15	1.940E−15
6	1	47	2	1.036E−23	3.753E−19	1.155E−17	6.197E−17	3.192E−16	1.119E−15	1.859E−15	2.659E−15
7	4	40	3	1.002E−23	9.276E−20	1.818E−18	7.811E−18	3.238E−17	9.658E−17	1.511E−16	2.088E−16
8	2	40	3	3.387E−24	3.162E−20	6.211E−19	2.672E−18	1.109E−17	3.311E−17	5.187E−17	7.179E−17
7	4	39	3	6.289E−24	5.238E−20	9.900E−19	4.175E−18	1.697E−17	4.969E−17	7.704E−17	1.055E−16
4	2	34	3	7.327E−24	6.276E−20	1.199E−18	5.088E−18	2.085E−17	6.167E−17	9.628E−17	1.330E−16
6	1	36	2	9.279E−24	7.476E−20	1.397E−18	5.855E−18	2.365E−17	6.886E−17	1.065E−16	1.455E−16
8	2	38	1	3.278E−24	2.632E−20	4.907E−19	2.054E−18	8.282E−18	2.409E−17	3.726E−17	5.100E−17
7	4	37	5	1.082E−23	8.116E−20	1.479E−18	6.121E−18	2.439E−17	7.020E−17	1.080E−16	1.470E−16
4	2	30	2	1.187E−23	9.201E−20	1.701E−18	7.097E−18	2.860E−17	8.351E−17	1.296E−16	1.782E−16
3	3	25	3	1.059E−24	7.892E−21	1.425E−19	5.845E−19	2.290E−18	6.415E−18	9.664E−18	1.286E−17
1	4	17	3	1.007E−23	7.484E−20	1.364E−18	5.654E−18	2.263E−17	6.571E−17	1.018E−16	1.397E−16
9	0	41	1	4.570E−23	3.583E−19	6.650E−18	2.783E−17	1.126E−16	3.301E−16	5.139E−16	7.089E−16
2	2	22	1	1.136E−23	8.316E−20	1.508E−18	6.231E−18	2.486E−17	7.200E−17	1.114E−16	1.526E−16
8	2	35	1	5.936E−24	4.313E−20	7.792E−19	3.214E−18	1.279E−17	3.691E−17	5.698E−17	7.800E−17
3	3	23	4	2.014E−23	1.433E−19	2.576E−18	1.060E−17	4.215E−17	1.218E−16	1.883E−16	2.582E−16
1	4	15	5	1.563E−23	1.092E−19	1.947E−18	7.973E−18	3.147E−17	9.015E−17	1.386E−16	1.889E−16
4	2	28	3	1.011E−23	7.061E−20	1.260E−18	5.168E−18	2.046E−17	5.887E−17	9.080E−17	1.242E−16
1	4	14	4	4.171E−24	2.861E−20	5.068E−19	2.069E−18	8.143E−18	2.327E−17	3.573E−17	4.867E−17
4	2	27	1	9.004E−24	6.406E−20	1.149E−18	4.723E−18	1.872E−17	5.384E−17	8.293E−17	1.132E−16
3	3	21	2	3.436E−24	2.378E−20	4.215E−19	1.718E−18	6.736E−18	1.909E−17	2.912E−17	3.937E−17
8	2	34	3	6.615E−24	4.622E−20	8.232E−19	3.368E−18	1.328E−17	3.793E−17	5.821E−17	7.920E−17
1	4	13	4	1.636E−23	1.086E−19	1.903E−18	7.730E−18	3.027E−17	8.615E−17	1.320E−16	1.795E−16
3	3	20	2	4.594E−24	3.078E−20	5.411E−19	2.201E−18	8.637E−18	2.464E−17	3.783E−17	5.156E−17
5	0	29	1	2.657E−23	1.727E−19	3.009E−18	1.220E−17	4.774E−17	1.362E−16	2.093E−16	2.856E−16
3	3	19	3	9.822E−24	6.462E−20	1.129E−18	4.580E−18	1.791E−17	5.092E−17	7.803E−17	1.061E−16
1	4	12	3	6.170E−24	3.904E−20	6.709E−19	2.692E−18	1.037E−17	2.897E−17	4.387E−17	5.890E−17
7	4	32	4	2.599E−23	1.671E−19	2.902E−18	1.174E−17	4.586E−17	1.306E−16	2.006E−16	2.737E−16
7	4	31	3	7.252E−24	4.551E−20	7.824E−19	3.146E−18	1.219E−17	3.434E−17	5.237E−17	7.088E−17
2	2	18	1	5.581E−24	3.495E−20	6.011E−19	2.419E−18	9.395E−18	2.660E−17	4.071E−17	5.536E−17
8	2	33	1	4.742E−24	3.085E−20	5.366E−19	2.170E−18	8.453E−18	2.392E−17	3.654E−17	4.952E−17
4	2	24	1	6.198E−24	4.066E−20	7.104E−19	2.882E−18	1.128E−17	3.216E−17	4.938E−17	6.731E−17
1	4	11	4	5.338E−24	3.267E−20	5.556E−19	2.218E−18	8.514E−18	2.372E−17	3.593E−17	4.829E−17
8	2	31	3	1.404E−23	8.905E−20	1.538E−18	6.204E−18	2.415E−17	6.854E−17	1.051E−16	1.431E−16
2	2	16	3	7.166E−24	4.264E−20	7.187E−19	2.858E−18	1.094E−17	3.046E−17	4.617E−17	6.218E−17
1	4	10	3	3.794E−24	2.168E−20	3.586E−19	1.408E−18	5.291E−18	1.437E−17	2.139E−17	2.826E−17
7	4	26	4	6.860E−24	3.659E−20	5.936E−19	2.313E−18	8.653E−18	2.359E−17	3.535E−17	4.712E−17

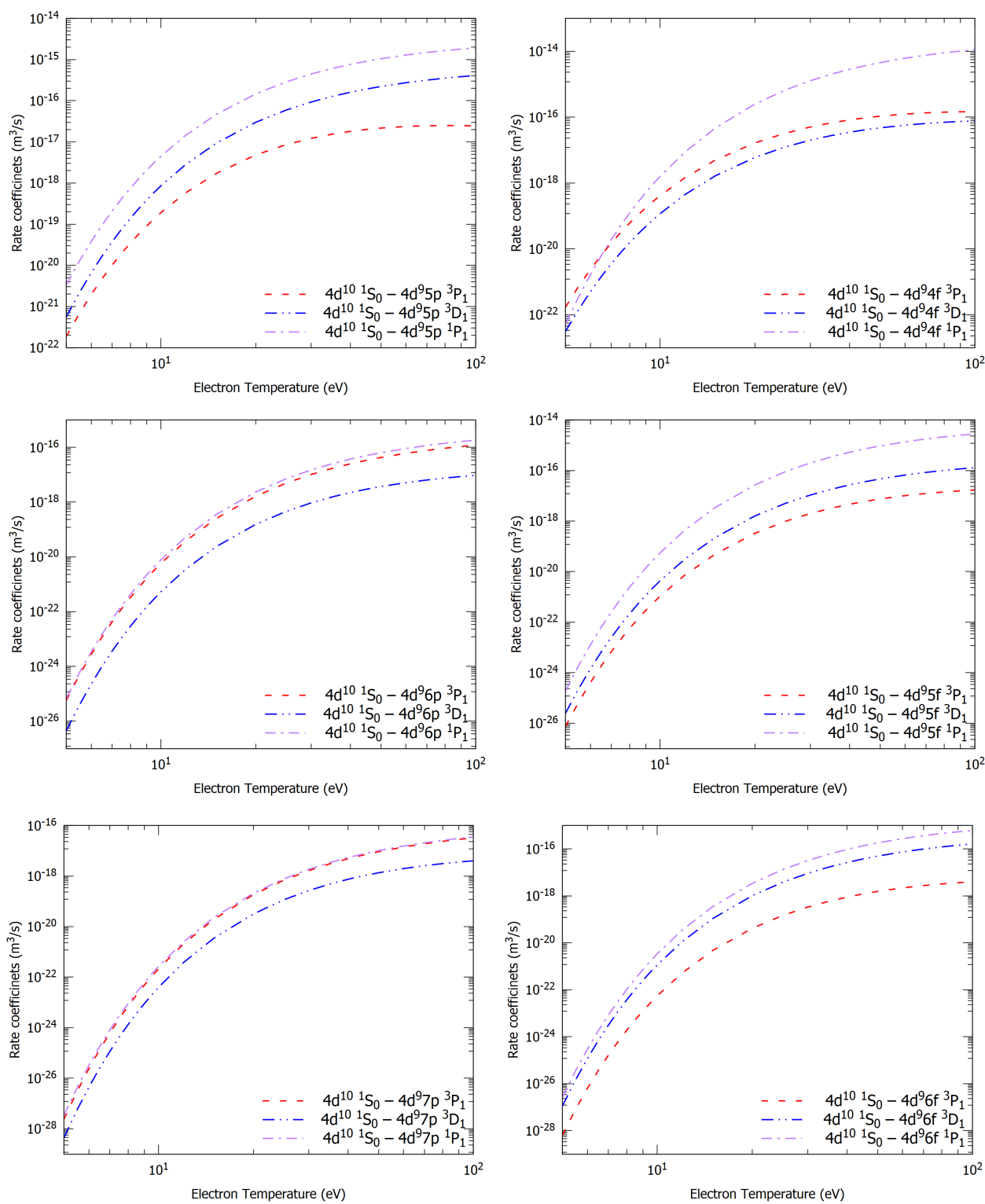


**Figure 2.** Excitation rate coefficients of  $Xe^{8+}$  as a function of electron temperature.

#### 4. Conclusions

We employed the MCDF approach within the framework of the Dirac–Coulomb Hamiltonian, including the Breit and QED corrections using the GRASP2K program [21] and calculated the energy levels, wavelengths and transition rates for the electric dipole allowed transitions of  $Xe^{7+}$ ,  $Xe^{8+}$ ,  $Xe^{9+}$  and  $Xe^{10+}$  ions in the EUV range of 8–19 nm. These results are compared with other reported experimental and theoretical results and, overall, a good agreement is found. After confirming the reliability of our ionic wavefunctions,

we used them in the RDW method to calculate the excitation cross sections for a total of 159 transitions in the four ions. To make our cross sections conveniently available for plasma modelling, we obtained the fitting parameters for these cross sections for both low and high incident electron energies. The maximum error in fitted cross sections is found to be well within 5% for most of the cases. Further, these cross sections are used to calculate the excitation rate coefficients for several electron temperatures ranging from 5 to 100 eV, assuming a Maxwellian electron energy distribution. Our cross sections and rate coefficients are reported for the first time, as no other experimental or theoretical results are available. We hope our results will be useful for the successful interpretation of EUV emissions from various sources.

**Supplementary Materials:** The following are available online at <https://www.mdpi.com/2218-2004/9/4/76/s1>, Table S1: Cross sections ( $10^{-20} \text{ m}^2$ ) for  $\text{Xe}^{7+}$  for the transitions from  $4d^{10}5s\ ^2S_{1/2}$  state at incident electron energies 200, 300, 400, 500, 700, 1000, 1200, 1500, 2000, 2500, 3000 eV. Table S2: Cross sections ( $10^{-20} \text{ m}^2$ ) for  $\text{Xe}^{8+}$  for the transitions from  $4d^{10}\ ^1S_0$  state at incident electron energies 200, 300, 400, 500, 700, 1000, 1200, 1500, 2000, 2500, 3000 eV. Table S3: Cross sections ( $10^{-20} \text{ m}^2$ ) for  $\text{Xe}^{9+}$  at incident electron energies 200, 300, 400, 500, 700, 1000, 1200, 1500, 2000, 2500, 3000 eV.  $a$  and  $b$  refer to the indices of the initial and final levels, respectively. Table S4: Cross sections ( $10^{-20} \text{ m}^2$ ) for  $\text{Xe}^{10+}$  at incident electron energies 200, 300, 400, 500, 700, 1000, 1200, 1500, 2000, 2500, 3000 eV.  $a$  and  $b$  refer to the indices of the initial and final levels, respectively.

**Author Contributions:** Both the authors have contributed equally in performing calculations and preparing the manuscript. All authors have read and agreed to the published version of the manuscript.

**Funding:** This research received no external funding.

**Institutional Review Board Statement:** Not applicable.

**Informed Consent Statement:** Not applicable.

**Data Availability Statement:** The data presented in this study are available in the article or supplementary material here.

**Acknowledgments:** Aloka Kumar Sahoo would like to acknowledge the Ministry of Human Resources and Development (MHRD) India for the award of a research fellowship.

**Conflicts of Interest:** The funders had no role in the design of the study; in the collection, analyses, or interpretation of data; in the writing of the manuscript, or in the decision to publish the results.

## References

1. Abramov, I.S.; Gospodchikov, E.D.; Shalashov, A.G. Extreme-Ultraviolet Light Source for Lithography Based on an Expanding Jet of Dense Xenon Plasma Supported by Microwaves. *Phys. Rev. Appl.* **2018**, *10*, 1. [[CrossRef](#)]
2. Werner, K.; Rauch, T.; Ringat, E.; Kruk, J.W. First detection of krypton and xenon in a white dwarf. *Astrophys. J.* **2012**, *753*, L7. [[CrossRef](#)]
3. Otsuka, M.; Tajitsu, A. Chemical abundances in the extremely carbon-rich and xenon-rich halo planetary nebula H4-1. *Astrophys. J.* **2013**, *778*, 146. [[CrossRef](#)]
4. Beattie, J.R.; Matossian, J.N. Xenon ion sources for space applications (invited). *Rev. Sci. Instruments* **1990**, *61*, 348–353. [[CrossRef](#)]
5. Churilov, S.S.; Joshi, Y.N. Analysis of the  $4p^64d^84f$  and  $4p^54d^{10}$  Configurations of Xe X and Some Highly Excited Levels of Xe VIII and Xe IX Ions. *Phys. Scr.* **2002**, *65*, 40–45. [[CrossRef](#)]
6. Churilov, S.S.; Joshi, Y.N.; Reader, J.; Kildiyarova, R.R.  $4p^64d^8 - (4d^75p + 4d^74f + 4p^54d^9)$  Transitions in Xe XI. *Phys. Scr.* **2004**, *70*, 126–138. [[CrossRef](#)]
7. Cowan, R.D. *The Theory of Atomic Structure and Spectra*; Number 3; University of California Press: Berkeley, CA, USA, 1981.
8. Fahy, K.; Sokell, E.; O’Sullivan, G.; Aguilar, A.; Pomeroy, J.M.; Tan, J.N.; Gillaspy, J.D. Extreme-ultraviolet spectroscopy of highly charged xenon ions created using an electron-beam ion trap. *Phys. Rev. A-At. Mol. Opt. Phys.* **2007**, *75*, 1–12. [[CrossRef](#)]
9. Ali, S.; Nakamura, N. High resolution EUV spectroscopy of xenon ions with a compact electron beam ion trap. *J. Quant. Spectrosc. Radiat. Transf.* **2017**, *198*, 112–116. [[CrossRef](#)]
10. Ali, S.; Nakamura, N. Extreme ultraviolet spectroscopy of highly charged xenon and barium with a compact electron beam ion trap. *Nucl. Instruments Methods Phys. Res. Sect. B Beam Interact. Mater. Atoms* **2017**, *408*, 122–124. [[CrossRef](#)]
11. Merabet, H.; Kondagari, S.; Bruch, R.; Fülling, S.; Hahto, S.; Leung, K.L.; Reijonen, J.; Godunov, A.L.; Schipakov, V.A. EUV emission from xenon in the 10–80 nm wavelength range using a compact ECR ion source. *Nucl. Instruments Methods Phys. Res. Sect. B Beam Interact. Mater. Atoms* **2005**, *241*, 23–29. [[CrossRef](#)]

12. Safronova, U.I.; Bista, R.; Bruch, R.; Merabet, H. Relativistic many-body calculations of atomic properties in Pd-like ions. *Can. J. Phys.* **2008**, *86*, 131–149. [[CrossRef](#)]
13. Ivanova, E.P. Energy levels in Ag-like ( $4d^{10}4f$ ,  $4d^{10}5l$  ( $l = 0\text{--}3$ )), Pd-like ( $4d^94f$  [ $J = 1$ ],  $4d^95p$  [ $J = 1$ ],  $4d^95f$  [ $J = 1$ ]), and Rh-like ( $4d^9$  [ $J = 5/2, 3/2$ ]) ions with  $Z \leq 86$ . *At. Data Nucl. Data Tables* **2009**, *95*, 786–804. [[CrossRef](#)]
14. Bokamba Motoumba, E.; Enzonga Yoca, S.; Quinet, P.; Palmeri, P. Ab initio MCDHF/RCI and semi-empirical HFR calculations of transition probabilities and oscillator strengths in Xe XI. *J. Quant. Spectrosc. Radiat. Transf.* **2019**, *235*, 217–231. [[CrossRef](#)]
15. Motoumba, E.B.; Yoca, S.E.; Palmeri, P.; Quinet, P. Relativistic Hartree–Fock and Dirac–Fock atomic structure and radiative parameter calculations in nine-times ionized xenon (Xe X). *J. Quant. Spectrosc. Radiat. Transf.* **2019**, *227*, 130–135. [[CrossRef](#)]
16. Shen, Y.; Gao, C.; Zeng, J. Electron impact collision strengths and transition rates for extreme ultraviolet emission from Xe $10+$ . *At. Data Nucl. Data Tables* **2009**, *95*, 1–53. [[CrossRef](#)]
17. Dressler, R.A.; hui Chiu, Y.; Zatsarinny, O.; Bartschat, K.; Srivastava, R.; Sharma, L. Near-infrared collisional radiative model for Xe plasma electrostatic thrusters: the role of metastable atoms. *J. Phys. D Appl. Phys.* **2009**, *42*, 185203. [[CrossRef](#)]
18. Gangwar, R.K.; Dipti; Srivastava, R.; Stafford, L. Spectroscopic diagnostics of low-pressure inductively coupled Kr plasma using a collisional–radiative model with fully relativistic cross sections. *Plasma Sources Sci. Technol.* **2016**, *25*, 035025. [[CrossRef](#)]
19. Gupta, S.; Gangwar, R.K.; Srivastava, R. Diagnostics of Ar/N<sub>2</sub> mixture plasma with detailed electron-impact argon fine-structure excitation cross sections. *Spectrochim. Acta Part B At. Spectrosc.* **2018**, *149*, 203–213. [[CrossRef](#)]
20. Baghel, S.S.; Gupta, S.; Gangwar, R.K.; Srivastava, R. Diagnostics of low-temperature neon plasma through a fine-structure resolved collisional–radiative model. *Plasma Sources Sci. Technol.* **2019**, *28*, 115010. [[CrossRef](#)]
21. Jönsson, P.; Gaigalas, G.; Bieroń, J.; Fischer, C.F.; Grant, I. New version: Grasp2K relativistic atomic structure package. *Comput. Phys. Commun.* **2013**, *184*, 2197–2203. [[CrossRef](#)]
22. Sharma, L.; Surzhykov, A.; Srivastava, R.; Fritzsche, S. Electron-impact excitation of singly charged metal ions. *Phys. Rev. A* **2011**, *83*, 062701. [[CrossRef](#)]
23. Kramida, A.; Ralchenko, Y.; Reader, J.; NIST ASD Team. *NIST Atomic Spectra Database* (ver. 5.8); National Institute of Standards and Technology: Gaithersburg, MD, USA, 2020. Available online: <https://physics.nist.gov/asd> (accessed on 21 August 2021)
24. Churilov, S.; Joshi, Y.N.; Reader, J. High-resolution spectrum of xenon ions at 13.4 nm. *Opt. Lett.* **2003**, *28*, 1478–1480. [[CrossRef](#)] [[PubMed](#)]
25. Bharti, S.; Sharma, L.; Srivastava, R. Electron impact excitation of Ge-like to Cu-like xenon ions in the extreme ultraviolet. *J. Phys. B At. Mol. Opt. Phys.* **2020**, *53*, 165001. [[CrossRef](#)]
26. Shukla, N.; Priti; Sharma, L.; Srivastava, R. Electron-impact excitations of highly charged tungsten ions and polarization study of their successive photon decay. *Eur. Phys. J. D* **2019**, *73*, 109. [[CrossRef](#)]
27. Priti.; Sharma, L.; Srivastava, R. Study of electron excitation of Rb-like to Br-like tungsten ions and polarization of their photon emission. *Eur. Phys. J. D* **2017**, *71*, 100. [[CrossRef](#)]
28. Das, T.; Sharma, L.; Srivastava, R. Electron impact excitation of the M-shell electrons from Zn-like through Co-like tungsten ions. *Phys. Scr.* **2012**, *86*, 035301. [[CrossRef](#)]
29. Dipti.; Das, T.; Sharma, L.; Srivastava, R. L-shell electron excitations of Mg- through O-like tungsten ions. *Phys. Scr.* **2014**, *89*, 085403. [[CrossRef](#)]
30. Dipti.; Das, T.; Sharma, L.; Srivastava, R. Electron impact excitation and polarization studies of Fe-like W $48+$  to Al-like W $61+$  ions. *Can. J. Phys.* **2015**, *93*, 888–897. [[CrossRef](#)]
31. Gangwar, R.K.; Sharma, L.; Srivastava, R.; Stauffer, A.D. C-R Model for Ar plasmas using reliable excitation cross-sections. *J. Physics: Conf. Ser.* **2012**, *388*, 042013. [[CrossRef](#)]
32. Dipti.; Gangwar, R.K.; Srivastava, R.; Stauffer, A.D. Collisional-radiative model for non-Maxwellian inductively coupled argon plasmas using detailed fine-structure relativistic distorted-wave cross sections. *Eur. Phys. J. D* **2013**, *67*, 203. [[CrossRef](#)]
33. Priti.; Dipti.; Gangwar, R.; Srivastava, R. Calculation of fully relativistic cross sections for electron excitation of cesium atom and its application to the diagnostics of hydrogen-cesium plasma. *J. Quant. Spectrosc. Radiat. Transf.* **2017**, *187*, 426–442. [[CrossRef](#)]
34. Priti.; Gangwar, R.K.; Srivastava, R. Collisional-radiative model of xenon plasma with calculated electron-impact fine-structure excitation cross-sections. *Plasma Sources Sci. Technol.* **2019**, *28*, 025003. [[CrossRef](#)]